Diverse origins of Arctic and Subarctic methane point source emissions identified with multiply-substituted isotopologues

Author links open overlay panel P.M.J.Douglas[a] D.A.Stolper[ab] D.A.Smith[ac] K.M.Walter Anthony[d] C.K.Paull[e] S.Dallimore[f] M.Wik[gh] P.M.Crill[gh] M.Winterdahl[hi] J.M.Eiler[a] A.L.Sessions[a]
Show more

Abstract

Methane is a potent greenhouse gas, and there are concerns that its natural emissions from the Arctic could act as a substantial positive feedback to anthropogenic global warming. Determining the sources of methane emissions and the biogeochemical processes controlling them is important for understanding present and future Arctic contributions to atmospheric methane budgets. Here we apply measurements of multiply-substituted isotopologues, or clumped isotopes, of methane as a new tool to identify the origins of ebullitive fluxes in Alaska, Sweden and the Arctic Ocean. When methane forms in isotopic equilibrium, clumped isotope measurements indicate the formation temperature. In some microbial methane, however, non-equilibrium isotope effects, probably related to the kinetics of methanogenesis, lead to low clumped isotope values. We identify four categories of emissions in the studied samples: thermogenic methane, deep subsurface or marine microbial methane formed in isotopic equilibrium, freshwater microbial methane with non-equilibrium clumped isotope values, and mixtures of deep and shallow methane (i.e., combinations of the first three end members). Mixing between deep and shallow methane sources produces a non-linear variation in clumped isotope values with mixing proportion that provides new constraints for the formation environment of the mixing end-members. Analyses of microbial methane emitted from lakes, as well as a methanol-consuming methanogen pure culture, support the hypothesis that non-equilibrium clumped isotope values are controlled, in part, by kinetic isotope effects induced during enzymatic reactions involved in methanogenesis. Our results indicate that these kinetic isotope effects vary widely in microbial methane produced in Arctic lake sediments, with non-equilibrium Δ_{18} values spanning a range of more than 5‰.

- **Previous** article
- **Next** article

Keywords

Methane
Clumped isotope geochemistry

Arctic

Carbon cycle

Greenhouse gases

1. Introduction

Methane (CH₄) is a critical atmospheric greenhouse gas, with 28 times (on a molar basis) the global warming potential of CO_2 on a 100-year timescale (Myhre et al., 2013). Due to its importance to the climate state of the Earth, the sources of methane to the atmosphere and how they might respond to future climate change are of key concern. One region where natural (i.e., non-anthropogenic) methane emissions are of interest and concern is the Arctic, which has been predicted to experience pronounced warming in the future (Holland and Bitz, 2003, Comiso and Hall, 2014). Methane emissions from Arctic environments have been predicted to increase under a warmer climate (Christensen et al., 2004, Walter et al., 2006, O'Connor et al., 2010, Walter Anthony et al., 2012, Thornton et al., 2015, Wik et al., 2016), thus acting as a positive feedback to global warming (Anisimov, 2007, Schuur et al., 2008, Schuur et al., 2015, Isaksen et al., 2011, Koven et al., 2011).

Microbial methanogenesis in wetland and lake sediments is thought to be the dominant source of natural methane emissions originating in the Arctic, contributing up to 90% of emissions during the boreal summer (Fisher et al., 2011). Consequently, this source has been the primary focus of studies of Arctic methane emissions (Walter et al., 2006, Schuur et al., 2008, Fisher et al., 2011, Isaksen et al., 2011). However, recent studies have identified two additional and potentially important sources of natural Arctic methane emissions. First, analyses of the isotopic and molecular composition of gases from ebullitive seeps in Alaskan lakes have suggested that many of these seeps emit methane from thermogenic or deep subsurface microbial sources. Such gases are thought to be transported to the surface by faults, and stored in shallow reservoirs underlying permafrost and glaciers (Walter Anthony et al., 2012). The emission of methane from these deep sources could be enhanced as permafrost thaws and glaciers melt, which could increase the number of conduits from subsurface reservoirs to the atmosphere (Formolo et al., 2008, Walter Anthony et al., 2012).

Second, methane ebullition has been observed in several locations on the continental shelf and slope of the Arctic Ocean (Paull et al., 2007, Westbrook et al., 2009, Shakhova et al., 2010). The sources of these bubbles may be from either the dissociation of gas hydrates or the thawing of permafrost inundated by sea level rise following the last deglaciation (Paull et al., 2007, Westbrook et al., 2009, Portnov et

al., 2013, Frederick and Buffett, 2014). Methane emitted from the Arctic Ocean shelf may not have a significant influence on atmospheric budgets, given evidence for its efficient oxidation in sediments and the water column (Graves et al., 2015, Overduin et al., 2015). Nevertheless, the source and distribution of methane emissions from the Arctic Ocean remain poorly constrained (Kort et al., 2012, Schuur et al., 2015), making it difficult to quantitatively evaluate the importance of these sources to the atmospheric methane budget.

Carbon and hydrogen stable isotope measurements are an important tool for fingerprinting different sources of methane (Schoell, 1980, Whiticar et al., 1986, Whiticar, 1999). For example, thermogenic methane typically contains greater $^{13}C/^{12}C$ and D/H ratios relative to microbial methane (Schoell, 1980). Additionally, stable isotope measurements can in some cases differentiate between pathways of microbial methanogenesis (Whiticar et al., 1986, Krzycki et al., 1987, Hornibrook et al., 1997, Hornibrook et al., 2000, Whiticar, 1999, Conrad et al., 2002, Krüger et al., 2002, Walter et al., 2008, Brosius et al., 2012). In particular, hydrogenotrophic methanogenesis (i.e., methanogens that reduce CO_2 with H_2) is thought to produce methane with lower $^{13}C/^{12}C$ and higher D/H relative to fermentative methanogenesis (i.e. methanogens that metabolize acetate or other methylated compounds) (Whiticar et al., 1986, Whiticar, 1999). However, ambiguities in the isotopic composition of methane can preclude accurate source assignment (Martini et al., 1996, Prinzhofer and Pernaton, 1997, Waldron et al., 1998, Waldron et al., 1999, Valentine et al., 2004, Conrad, 2005). For example, microbial methanogenesis in some environments can produce stable isotope compositions resembling thermogenic methane (Martini et al., 1996, Valentine et al., 2004). Additionally, multiple factors in addition to methanogenic pathway can substantially influence the stable isotope composition of microbial methane, including substrate isotopic composition, substrate limitation, the kinetics of methane production, transport, and oxidation (Sugimoto and Wada, 1995, Waldron et al., 1998, Waldron et al., 1999, Whiticar, 1999, Valentine et al., 2004, Conrad, 2005, Penning et al., 2005). These multiple influences on methane stable isotope values can complicate inferences regarding the pathway of methanogenesis in natural samples (Conrad, 2005).

Recently the analysis of multiply-substituted isotopologues, or 'clumped isotopes', has emerged as an additional isotopic constraint on the sources of methane (Tsuji et al., 2012, Ono et al., 2014, Stolper et al., 2014a, Stolper et al., 2014b, Inagaki et al., 2015, Stolper et al., 2015, Wang et al., 2015). Clumped-isotope geochemistry refers to the analysis of the abundances of molecules containing multiple rare, heavy isotopes (e.g. $^{13}CH_3D$ and $^{12}CH_2D_2$). Clumped isotope analyses are of interest in part because the

proportions of clumped isotope species in equilibrated systems are solely a function of temperature-dependent homogeneous [phase equilibria](#) ([Urey and Rittenberg, 1933](#), [Wang et al., 2004](#)) and can be used to determine formation or re-equilibration temperatures of a molecule using only a single phase, as opposed to multiple phases as is typical in stable-isotope-based [geothermometry](#)([Eiler and Schauble, 2004](#), [Ghosh et al., 2006](#), [Stolper et al., 2014a](#), [Stolper et al., 2014b](#)). See [Eiler, 2007](#), [Eiler, 2011](#), [Eiler, 2013](#), and references therein for detailed reviews of clumped-isotope geochemistry.

The first accurate and precise clumped isotope measurements of methane were achieved on a prototype high-resolution [isotope ratio](#) mass spectrometer—the Thermo Fisher IRMS 253 Ultra (hereafter the 'Ultra') ([Eiler et al., 2013](#)). Most measurements of methane clumped isotopes performed with the Ultra report variations in the sum of $^{13}CH_3D$ and $^{12}CH_2D_2$, as measured by the quantity Δ_{18} ([Stolper et al., 2014a](#)). Δ_{18} values represent the relative deviation in a sample from the amount of mass-18 methane predicted for a [random distribution](#)of isotopes among all isotopologues of the sample (for more details see Section [2.5](#)). Δ_{18} values primarily reflect the anomaly in $^{13}CH_3D$, which makes up ~98% of the mass-18 isotopologues in naturally-occurring methane ([Stolper et al., 2014a](#)). In systems that are in internal isotopic equilibrium, the Δ_{18} value is a unique function of the sample's formation or re-equilibration temperature ([Stolper et al., 2014a](#), [Stolper et al., 2014b](#)), and is particularly useful in differentiating high temperature thermogenic from low temperature microbial methane (e.g. [Stolper et al., 2015](#)).

Mixing of gases that differ in their conventional isotopic composition (i.e., $^{13}C/^{12}C$ and D/H) can produce non-linear variations in clumped isotope indices (including Δ_{18}) ([Fig. 1](#)) ([Eiler and Schauble, 2004](#), [Eiler, 2007](#)). Such mixing effects have been studied for CO_2, O_2, and CH_4 and have contributed to the understanding of gas mixing in natural samples ([Affek and Eiler, 2006](#), [Yeung et al., 2012](#), [Stolper et al., 2014b](#), [Stolper et al., 2015](#)). In poorly constrained cases these mixing effects can complicate clear interpretation of clumped isotope signals, and could be misinterpreted as incorrect formation temperatures. When clumped isotope data are combined with other isotopic or gas composition data, however, this phenomenon becomes a potentially powerful tool to recognize mixing and constrain the properties and relative proportions of end members in mixed gases.
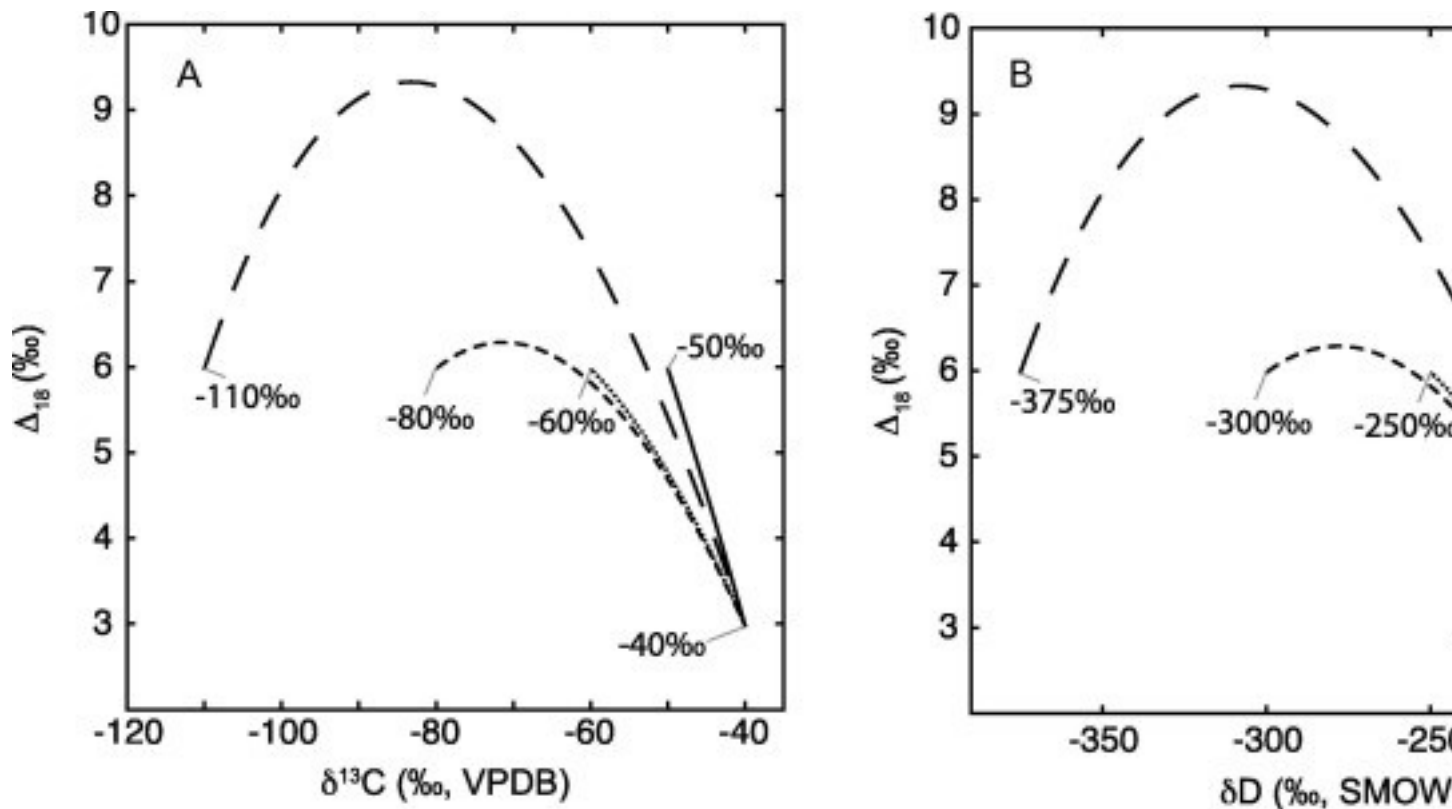
Fig. 1. Hypothetical examples of non-linear mixing effects for Δ_{18} values. Plots show mixing relationships in $\delta^{13}C$–Δ_{18} space (A) and δD–Δ_{18} space (B) for mixtures of [methane](#) with varying end-member compositions. In these examples the end-member Δ_{18} values remain fixed at 3‰ and 6‰, but the $\delta^{13}C$ and δD values of the isotopically light end-member varies. End-member $\delta^{13}C$ and δD values are denoted on the plots. For mixtures where $\delta^{13}C$ and δD values are relatively similar, mixing in Δ_{18} is approximately linear (solid line); as the $\delta^{13}C$ and δD values of the mixing end-members become increasingly widely spaced the [non-linearity](#) of mixing in Δ_{18} becomes more pronounced (dashed lines).

In some situations, clumped-isotope values of CO_2, carbonate minerals, O_2, and CH_4 have been shown to deviate from their thermodynamically predicted equilibrium value in materials where the formation temperature is known or well-constrained ([Ghosh et al., 2006](#), [Affek et al., 2007](#), [Affek et al., 2008](#), [Kluge and Affek, 2012](#), [Saenger et al., 2012](#), [Stolper et al., 2014b](#), [Stolper et al., 2015](#), [Wang et al., 2015](#), [Yeung et al., 2015](#)). These non-equilibrium clumped isotope values are generally thought to be related to kinetic [isotope effects](#) ([Kluge and Affek, 2012](#), [Affek and Zaarur, 2014](#), [Stolper et al., 2015](#), [Wang et al., 2015](#), [Yeung et al., 2015](#)), and preclude, or at least complicate, the

accurate identification of sample formation temperatures. At the same time, non-equilibrium clumped isotope signatures have the potential to provide valuable new information about chemical kinetics and biochemical reaction pathways (Passey, 2015, Stolper et al., 2015, Wang et al., 2015, Yeung et al., 2015).

This paper provides a focused application of clumped isotope analyses to understand the origin of methane emitted from natural point sources in the Arctic, with a focus on methane bubble fluxes from lakes in Alaska and Sweden and from the Beaufort Sea in the Arctic Ocean. In addition to providing new insights into the methane budgets of these locations, this study provides an example of how methane clumped-isotope analyses can be used to understand and quantify the sources of methane emissions in natural environments. We focus on two key applications of clumped isotopes. First, we apply this technique to differentiate the contributions of microbial and thermogenic methane to ebullitive methane fluxes. Second, we explore the factors controlling the clumped-isotope values of microbial methane emitted in Arctic environments. We also present an analysis of methane produced by a methanogen pure culture consuming a methanol substrate, which provides insights into the clumped isotope signature of fermentative pathways of methanogenesis.

2. Methods

2.1. Study sites

We analyzed a total of 26 samples from 12 lakes and 3 marine localities (Table 1, Fig. 2). Samples were chosen to include a diverse set of Arctic environments with differences in methaneflux and conventional stable isotope geochemistry. In particular, we selected some samples that were likely to contain thermogenic methane, as indicated by conventional stable isotope, radiocarbon, and gas composition measurements (Walter Anthony et al., 2012).

Table 1. Sample location, $[C_1]/[C_2]$, CH_4 flux, and CO_2 and H_2O isotope data.

Sample	Region	Latitude (°N)	Longitude (°E)	$[C_1]/[C_2]$[a]	CH_4flux[b]	1σ	$\delta^{13}C$ CO_2(‰, VPDB)	Estimated H_2O δD (‰, VSMOW)	1σ
Cake Eater	North Slope	71.28	−156.64	*nd*	0.017[c]		−23.39	−135[h]	16
Sukok	North Slope	71.07	−156.82	655	39.48[c]		−27.35	n/a	
Lake Q	North Slope	70.38	−157.35	*nd*	93400[d]		−37.76	n/a	

Sample	Region	Latitude (°N)	Longitude (°E)	$[C_1]/[C_2]$[a]	CH_4 flux[b]	1σ	$\delta^{13}C$ CO_2(‰, VPDB)	Estimated H_2O δD (‰, VSMOW)	1σ
Killarney	Fairbanks	64.87	−147.90	*na*	2.5[e]	1.81	−19.82	n/a	
Goldstream-Hotspot	Fairbanks	64.92	−147.85	*na*	6.5[e]	4.7	−19.22	−210[j]	30
Goldstream-Tiny	Fairbanks	64.92	−147.85	*nd*	0.116[e]		−17.28	−186[j]	30
Goldstream-A	Fairbanks	64.92	−147.85	*na*	0.005[e]	0.005	−24.12	−156[k]	30
Doughnut	Fairbanks	64.90	−147.91	145	25.9[f]	21.28	−4.07	−210[j]	30
Smith-Hotspot	Fairbanks	64.87	−147.87	*nd*	6.7[e]	4.87	−11.03	−156[k]	30
Eyak-1	SE Alaska	60.56	−145.67	35,700	0.50[c]		−8.97	n/a	
Eyak-2	SE Alaska	60.56	−145.67	224,000	1.3[c]		−12.9	n/a	
Eyak-3	SE Alaska	60.56	−145.67	137,500	0.51[c]		−10.39	n/a	
Prince William Sound	SE Alaska	60.59	−145.70	*na*	nd		n/a	n/a	
Katalla	SE Alaska	60.18	−144.44	*nd*	66.2[c]		−37.86	n/a	
ROV 38 m	Beaufort	70.48	−136.48	11,800	nd		n/a	−15[l]	14
Core 400 m	Beaufort	70.48	−136.48	2310	nd		n/a	−40[m]	4
ROV 420 m	Beaufort	70.79	−135.57	5930	nd		n/a	−40[m]	4
Inre Harrsjön Trap 10	Stordalen	68.36	19.05	*na*	5.14[c]		n/a	−94[n]	2
Inre Harrsjön Trap 4	Stordalen	68.36	19.05	*na*	4.46[c]		n/a	−94[n]	2
Inre Harrsjön Trap 6	Stordalen	68.36	19.05	*na*	9.16[c]		n/a	−94[n]	2
Mellersta Harrsjön Trap 21	Stordalen	68.36	19.04	*na*	1.54[g]		n/a	−94[n]	2
Mellersta Harrsjön Trap 19	Stordalen	68.36	19.04	*na*	8.34[c]		n/a	−94[n]	2
Mellersta	Stordalen	68.36	19.04	*na*	183.54[c]		n/a	−94[n]	2

Sample	Region	Latitude (°N)	Longitude (°E)	$[C_1]/[C_2]$[a]	CH_4flux[b]	1σ	$\delta^{13}C$ CO_2(‰, VPDB)	Estimated H_2O δD (‰, VSMOW)	1σ
Harrsjön Trap 24									
Villasjön Trap 34	Stordalen	68.35	19.05	*na*	29.8[c]		n/a	−70[g]	1
Villasjön Trap 31,34,35	Stordalen	68.35	19.05	*na*	3.77[c]		n/a	−70[g]	1
Villasjön Trap 31	Stordalen	68.35	19.05	*na*	41.41[c]		n/a	−70[g]	1

a

nd: ethane not detected; *na*: ethane concentration not analyzed.

b

Flux estimates for Alaskan samples are in units of L trap^{-1} day^{-1}; for the Stordalen samples they are in units of L m^{-2} day^{-1}.

c

Flux estimate specific to gas analyzed.

d

Flux measured from the same seep on a different day than gas sampling.

e

Based on average gas flux for seep class (Hotspot, Tiny, and A-type; Walter Anthony and Anthony, 2013, Lindgren et al., 2016).

f

Average flux measured between August and October 2011.

g

Trap specific average flux over six years of measurements.

h

Estimate based on texture ice δD value in the vicinity of the lake (Meyer et al., 2010). Texture ice is inferred as a likely source of methane formation water given Holocene ^{14}C age of texture-ice organics and the methane sample (Table 2).

i

Estimate based on Pleistocene ice wedge δD values ([Brosius et al., 2012](#)). Pleistocene ice wedges are inferred as a likely source of methane formation water given the Pleistocene age of this methane sample ([Table 2](#)).

j

Estimate is an average of Pleistocene ice wedge and Holocene ground ice δD values ([Brosius et al., 2012](#)). The location of these seeps suggests that pore waters include input of thawed ice from both sources.

k

Estimate based on Holocene ground ice δD values ([Brosius et al., 2012](#)). Holocene ice wedges are inferred as a likely source of methane formation water given the Holocene age of these methane samples ([Table 2](#)).

l

Estimate based on average δD of pore water samples in the vicinity of methane sampled from vents and sediments ([Paull et al., 2011](#)).

m

Estimate based on average δD of pore water samples in the vicinity of the sampled gas vent ([Paull et al., 2015](#)).

n

Estimate based on average δD of water samples from Mellersta Harrsjön ($n = 10$).

o

Estimate based on average δD of water samples from Villasjön ($n = 15$).

■ North Slope Alaska   ◆ Beaufort Sea

▲ Fairbanks Alaska   ▽ Stordalen Sweden

● Southeast Alaska

1. Download high-res image (473KB)
2. Download full-size image

Fig. 2. Map of the Arctic showing the location of the studied methanesamples (the base map is an open access file from Wikimedia).

We analyzed ebullitive gas samples from three lakes on the North Slope of Alaska (Lake Sukok, Lake Q, and Cake Eater Lake; Table 1, Fig. 2), a region with a large number of shallow thermokarst lakes (lakes formed by the thaw of ice-rich permafrost). This region contains active oil and gas production, and is also underlain by shallow coal seams (Walter Anthony et al., 2012).

We analyzed a total of six ebullitive gas samples from four lakes in the vicinity of Fairbanks, AK (Goldstream Lake, Killarney Lake, Smith Lake, and Doughnut Lake; Table 1, Fig. 2). All of these lakes were formed by thermokarst erosion, and one of them (Goldstream Lake) is actively eroding yedoma-type permafrost, a variety of loess permafrost that is rich in organic carbon (Walter et al., 2006, Brosius et al., 2012).

We analyzed five ebullitive gas samples from southeast Alaska (Table 1, Fig. 2), including three samples from Eyak Lake, a shallow coastal lake next to Cordova, AK. One sample is from Prince William Sound (PWS), in close vicinity to Eyak Lake, and one sample is from a stream in the vicinity of Katalla, AK, about 80 km to the east of Eyak Lake.

We analyzed nine ebullitive gas samples from three intensively studied, post-glacial lakes (Inre Harrsjön, Mellersta Harrsjön, and Villasjön), within the Stordalen Mire complex, a Subarctic peatland underlain by sporadic permafrost in northern Sweden (Table 1, Fig. 2) (Wik et al., 2013).

Finally, we analyzed three samples from the continental shelf and slope of the Beaufort Sea in the Arctic Ocean (Table 1, Fig. 2). Two samples were collected from an elevated topographic feature at a water depth of 420 m (Paull et al., 2015). One of these samples was collected from gas bubbles emitted from an active gas vent, and the other from a gas expansion void in a sediment core collected adjacent to the vent. One sample was collected from gas bubbles emitted from an elevated topographic feature at a water depth of 38 m on the continental shelf (Paull et al., 2011).

2.2. Sample collection

Ebullitive gas samples from Alaskan lakes were collected from submerged, umbrella-style gas bubble traps, following methods described by Walter et al. (2008), between 2009 and 2013. As discussed in Appendix 1, repeat isotopic analyses of these samples did not indicate analytical artifacts related to their storage. Bubble traps were fixed in place over discrete points of concentrated gas bubbling. Gas bubble samples from the Stordalen lakes were collected using submerged inverted funnels, as described by Wik et al. (2013), in June and July of 2014. These traps were part of a stratified sampling scheme but were not fixed over previously identified points of gas, as no sites of continuous, coherent bubbling were identified in the Stordalen lakes. All lake ebullitive gas samples were transferred to glass serum vials and sealed with crimped butyl rubber stoppers.

The ebullitive gas sample from the Beaufort shelf vent (38 m water depth) was collected by a Phantom S2 remotely operated vehicle (ROV) using a gas collection funnel and sampling system in 2010, as described in Paull et al. (2011). This gas sample was transferred underwater to a glass serum vial sealed with a butyl stopper. The gas bubble sample from the Beaufort slope vent (420 m water depth) was collected by the Monterey Bay Aquarium Research Institute (MBARI) miniROV using a gas collection funnel and sampling system in 2012, as described in Paull et al. (2015). This gas sample was transferred underwater to a stainless steel cylinder. The Beaufort slope sediment gas sample was collected by sampling a gas expansion void within a gravity core collected at 400 m water depth in 2012 (Paull et al., 2015). Gas was sampled through the core lining using a gas-tight syringe, and was stored in a glass serum bottle sealed with a butyl stopper.

2.3. Culture preparation

A pure culture of Methanosarcina acetivorans (Sowers et al., 1984; Strain DSM 2834; DSMZ GmbH) was grown on a carbon substrate of methanol in a 1 L glass serum bottle. It was grown under a headspace of N_2 gas, at a pressure of 150 kPa, in sterile media (~350 mL) containing (g/L): NaCl (23.4), $MgSO_4 \cdot 7\ H_2O$ (9.44), $NaHCO_3$ (5.0), KCl (0.8), NH_4Cl (1.0), Na_2HPO_4(0.6), $CaCl_2 \cdot 2\ H_2O$ (0.14), cysteine-HCl (0.25), with the addition of 10 mL DSM 141 Trace Element solution and 10 mL of DSM 141 Vitamin solution, 5 mL 99.9% MeOH, and 2.5 mL of a 50 mM H_2S^- solution. The culture bottle was kept in an incubator at 28 °C and shaken at 35 revolutions per min. Two aliquots of the headspace gas were sampled after 20 days of growth for methane purification and analysis.

Filter-sterilized media water was sampled at the same time as methane, and the δD value was measured using a spectroscopic DLT-100 Liquid-Water Isotope Analyzer (Los Gatos Research Inc.), with a precision of ~<1‰ (Feakins and Sessions, 2010). The $\delta^{13}C$ of methanol from the same supply as the culture media was measured by combusting an aliquot in a sealed tubed with cupric oxide at 800 °C, and then measuring the $\delta^{13}C$ value of the resulting CO_2 using Finnigan 252 isotope ratio mass spectrometer. We also derivatized a disodium phthalate standard with a known δD value (−95.3 ± 1.2‰; from A. Schimmelmann, University of Indiana) using methanol from the same supply as the culture media, and using acetyl chloride as the derivatizing agent. We then analyzed the δD value of the resulting phthalic acid methyl ester using a ThermoFinnigan Trace gas chromatograph coupled to a Delta[plus]XP isotope ratio mass spectrometer via a pyrolysis interface (Jones et al., 2008), with a typical precision of

∼<5‰. We calculated the δD value of the methanol methyl-group hydrogen by mass balance.

2.4. Methane purification

Methane (CH_4) was purified from mixed gas samples using the methods described previously by Stolper et al., 2014a, Stolper et al., 2014b. For all analyses we sampled enough gas to obtain approximately 50 μmol of CH_4. Gases were sampled from sealed glass vials and the culture serum bottle using a 5 ml gas tight syringe (Hamilton). The gas from the steel cylinder was sampled by connecting the cylinder to the vacuum line as described in Stolper et al. (2014a) with a Swagelok™ fitting. Gas samples were first exposed to liquid nitrogen to trap H_2O, CO_2, and H_2S. The gases in the headspace (including CH_4, O_2, and N_2) were then exposed and transferred to a 20 K cold trap, cooled using a helium cryostat (Janis Research). At this point residual gases, including He and H_2, were pumped away. The cold trap was then sealed, heated to 80 K, cooled to 45 K, and opened to vacuum to remove N_2 and O_2. This step was repeated until <2.67 Pa of gas remained in the cold trap at 45 K, corresponding to a purity of CH_4 of ∼99.8% (Stolper et al., 2014b). The cryostat was then heated to 70 K, and CH_4 was transferred to a Pyrex™ breakseal containing molecular sieve (EM Science; type 5A) immersed in liquid N_2. Prior to introduction to the mass spectrometer dual inlet, samples were heated with either a heat gun or a heated copper block set to ∼150 °C for 2–3 h to ensure minimal isotopic fractionation when transferring CH_4 from the molecular sieves (Stolper et al., 2014a).

2.5. Methane stable isotope measurements

Methane δD, $δ^{13}C$, and $Δ_{18}$ were measured using the Ultra, as described in detail by Stolper et al. (2014a). δD and $δ^{13}C$ values are expressed using delta notation relative to Vienna Standard Mean Ocean Water (VSMOW) and Vienna Pee Dee Belemnite (VPDB), respectively:

$$(1) \quad δD = \frac{^2R_{sample} - ^2R_{VSMOW}}{^2R_{VSMOW}}$$

$$(2) \quad δ13C = \frac{^{13}R_{sample} - ^{13}R_{VPDB}}{^{13}R_{VPDB}}$$

where ^2R and ^{13}R are the ratios D/H and $^{13}C/^{12}C$ respectively. δD and $δ^{13}C$ data are expressed as per mil (‰) values (Coplen, 2011).

Clumped isotope compositions are expressed using $Δ_{18}$ notation (Stolper et al., 2014a):

$$(3) \quad Δ18 = (18R/18R* - 1)$$

where

$$(4) \quad 18R = ([13CH3D] + [12CH2D2])/[12CH4]$$

The specified isotope ratios are measured from the corresponding ion [beam current](#) ratios, standardized by comparison with a standard of known composition. $^{18}R*$ is the ^{18}R value expected for a random internal distribution of isotopologues, given the $\delta^{13}C$ and δD values of the sample ([Stolper et al., 2014a](#)), and is expressed as:

$$(5) \quad {}^{18}R* = 6 \times [{}^2R]^2 + 4 \times {}^2R \times {}^{13}R$$

The factors ('6' and '4') in Eq. [(5)](#) derive from the symmetry numbers of the mass 18 methane isotopologues ([Stolper et al., 2014a](#)). Δ_{18} data are reported as per mil (‰), where 0‰ refers to a [random distribution](#) of methane isotopologues (i.e., $^{18}R = {}^{18}R*$). All samples are referenced against a laboratory standard with a Δ_{18} value of 2.981 ± 0.015‰, as described by [Stolper et al. (2014a)](#). Δ_{18} values can be related to equivalent formation temperature (K), assuming formation in internal isotopic equilibrium, via the equation ([Stolper et al., 2014a](#)):

$$(6) \quad \Delta_{18} = -0.0117106 T^2 + 0.708106 T^2 - 0.337$$

Because the Δ_{18}–T relationship is not linear, the error for inferred temperatures are not symmetric. 2σ errors for inferred temperatures reported in [Table 2](#) are the average of the upper and lower errors. For the samples for which the inferred temperatures are relevant in this study (i.e. samples inferred to have formed in internal isotopic equilibrium), the difference between upper and lower errors are at most 4 °C, and this asymmetry does not affect our interpretations.

Table 2. [Methane](#) isotope data.

Sample	n	δD (‰, VSMOW)	2 SE	$\delta^{13}C$ (‰, VPDB)	2 SE	Δ_{18}(‰)[a]	2 SE	Inferred temperature (°C)[b]	2 SE[c]	$\Delta^{14}C$ (‰)
Cake Eater	2	−371.4	0.22	−64.00	0.01	−0.4	0.45	n/a		−394.3
Sukok	1	−193.1	0.20	−46.31	0.01	4.1	0.46	102	23	−997.6
Lake Q	1	−238.3	0.24	−59.31	0.01	6.8	0.50	9	14	−1000
Killarney	2	−312.5	0.66	−88.76	0.01	9.6	0.66	*−61*	15	−907.7
Goldstream-Hotspot	2	−383.1	0.26	−77.59	0.26	2.0	0.70	*268*	91	−971.2
Goldstream-Tiny	1	−369.3	0.24	−64.34	0.01	1.1	0.44	*412*	130	nd
Goldstream-A	1	−332.8	0.24	−61.89	0.01	0.2	0.46	*905*	n/a	−314.9
Doughnut	1	−302.4	0.24	−55.50	0.01	6.0	0.48	29	16	−984.1
Smith-Hotspot	1	−362.2	0.24	−62.73	0.01	0.7	0.50	*549*	246	−265.3
Eyak-1	2	−172.4	0.34	−46.81	0.08	6.2	0.48	24	14	−851.0
Eyak-2	2	−203.5	0.26	−60.74	0.02	9.1	0.80	*−47*	19	nd

Sample	n	δD (‰, VSMOW)	2 SE	δ¹³C (‰, VPDB)	2 SE	Δ_{18}(‰)[a]	2 SE	Inferred temperature (°C)[b]	2 SE[c]	$\Delta^{14}C$ (‰)
Eyak-3	2	−242.6	0.24	−73.83	0.01	8.4	0.50	*−31*	12	−384.4
Prince William Sound	2	−151.0	0.24	−34.34	0.08	4.8	0.50	73	20	nd
Katalla	1	−171.0	0.22	−40.80	0.01	6.1	0.48	27	15	−987.1
ROV 38 m	2	−228.6	1.30	−83.02	0.04	6.9	0.43	5	11	−997.0
Core 400 m	1	−212.1	0.24	−65.32	0.01	7.1	0.44	0	11	nd
ROV 420 m	2	−210.3	0.24	−65.21	0.12	6.9	0.46	5	12	−995.0
Inre Harrsjön Trap 10	1	−310.3	0.22	−68.04	0.01	2.8	0.43	*187*	35	nd
Inre Harrsjön Trap 4	1	−285.9	0.23	−77.61	0.01	5.4	0.49	*50*	17	nd
Inre Harrsjön Trap 6	1	−311.6	0.25	−68.28	0.01	1.9	0.49	*271*	65	nd
Mellersta Harrsjön Trap 21	1	−288.1	0.21	−71.03	0.01	4.4	0.44	*90*	20	nd
Mellersta Harrsjön Trap 19	1	−282.2	0.23	−68.01	0.01	4.6	0.45	*79*	19	nd
Mellersta Harrsjön Trap 24	1	−293.1	0.25	−68.01	0.01	5.0	0.48	*64*	18	nd
Villasjön Trap 34	1	−300.7	0.21	−65.49	0.01	3.7	0.50	*126*	28	nd
Villasjön Trap 31,34,35	1	−314.9	0.23	−66.60	0.01	2.5	0.45	*215*	44	nd
Villasjön Trap 31	1	−312.7	0.25	−62.32	0.01	1.8	0.47	*291*	69	nd
Methanosarcina acetivorans[d]	2	−346.7	0.28	−30.23	0.16	−5.4	0.46	n/a		nd

a

Values relative to stochastic distribution of isotopologues.

b

Italics denote temperatures inferred to be implausible for methane formation for a given sample, which reflect mixing or non-equilibrium isotope effects.

c

Errors for inferred temperatures are average of upper and lower temperature estimates since Δ_{18}–T relationship is not linear.

    d

Grown at 28 °C.

The samples were analyzed over the course of 5 separate measurement periods of 2–15 weeks in duration, spanning 14 months in total. These measurement periods were separated by intervals of time when the Ultra was used for other measurements. Ten of the samples analyzed for this study were analyzed as replicates, in some cases in multiple measurement periods. We present measurement uncertainties for individual samples as either two standard errors of the internal measurement variability for a single measurement (2 SE), or 2 SE of replicate measurements. Reported uncertainties for inferred temperatures are propagated from the 2 SE errors for Δ_{18} values using Eq. (6). External reproducibility for Δ_{18}, δD, and $δ^{13}C$ values (1 σ) was 0.38‰, 0.22‰ and 0.06‰ respectively. A more detailed description of standardization and external reproducibility is provided in Appendix 2.

2.6. Other isotope measurements

Carbon isotopes of CO_2 contained in gas bubbles from the Alaskan lakes were measured at Florida State University, as described by Walter Anthony et al. (2012). Methane radiocarbon abundance for the Alaskan lake and Beaufort Sea samples was measured by accelerator mass spectrometry (AMS) at either the Woods Hole Oceanographic Institution's National Ocean Sciences AMS facility or the University of California at Irvine Keck Carbon Cycle AMS facility (Paull et al., 2011, Paull et al., 2015, Brosius et al., 2012, Walter Anthony et al., 2012). Radiocarbon data are expressed as $\Delta^{14}C$ in per mil notation (Stuiver and Polach, 1977):

$$(7) \quad \Delta 14C = Fm * e\lambda(1950\text{-}Yc)\text{-}1$$

where Fm is the deviation of the sample $^{14}C/^{12}C$ ratio relative to 95% of the $^{14}C/^{12}C$ ratio of the NBS Oxalic Acid standard in the year 1950, λ is 1/8267 (the reciprocal of the mean-life of ^{14}C), and Yc is the year the sample was collected.

To estimate the δD value of methane formation water for the Alaskan and Beaufort Sea samples we relied on published data for the isotopic composition of pore water or permafrost ice from either the studied sites (when possible), or same region of Alaska (Table 1) (Meyer et al., 2010, Paull et al., 2011, Paull et al., 2015, Brosius et al., 2012). For the Stordalen Mire samples we applied δD values measured in lake water samples. Grab samples for water isotope analyses were collected from Mellersta Harrsjön (10 samples) and Villasjön (15 samples) in acid washed 50 ml polyethylene bottles in

August 2005 and samples were stored cool to avoid evaporation before analysis. Water samples were reduced to H_2 using chromium oxidation using a Finnigan H-device, and δD values were measured with a Finnigan Delta V isotope-ratio mass spectrometer at the Stable Isotope Laboratory at the Department of Geological Sciences, Stockholm University, with a typical precision of ±2‰. Average δD values and standard deviations for each lake are reported in Table 1. We applied water δD measurements from Mellersta Harrsjön to samples from Inre Harrsjön since these two lakes have similar physiographic characteristics (Wik et al., 2013). As there are differences in the source of water isotope data between study sites, we apply the largest standard deviation associated with water δD measurements (±30‰ for measurements of Fairbanks area ice wedges; Brosius et al., 2012) as a conservative estimate of uncertainty for methane formation water δD.

We calculated apparent carbon dioxide–methane ($13αCO2$-CH4) and water-methane ($2αH2O$-CH4) isotopic fractionation factors using the equations:

(8) $13αCO2$-CH4=$13RCO2/13RCH4$

(9) $2αH2O$-CH4=$2RH2O/2RCH4$

Propagated errors for α values were calculated using the individual errors for isotope measurements of CH_4, CO_2, and H_2O.

2.7. Gas concentration and flux measurements

The concentrations of methane and other gases in the Alaskan lake samples were measured at the University of Alaska Fairbanks, as described in Walter Anthony et al. (2012). In some samples, ethane concentrations were analyzed using the same methodology, and were used to calculate $[C_1]/[C_2]$ ratios (Table 1). Gas ebullition fluxes (L gas day^{-1} trap^{-1}; Table 1) were measured via gas volume accumulations in bubble traps either manually or using data loggers over periods ranging from 20 min to 47 days (Walter Anthony et al., 2012). In Alaska all samples were collected from identified gas seeps, and therefore flux estimates were not dependent on the area of the traps. For some seeps reported gas fluxes are estimates based on measurements of seeps from the same region of Alaska with similar characteristics (Table 1). Gas composition analyses for the Beaufort Sea samples were performed by Isotech Laboratories (Paull et al., 2011, Paull et al., 2015).

Methane concentrations in the Stordalen lake samples were measured at the Abisko Scientific Research Station (Wik et al., 2013). Gas fluxes were estimated by measuring gas volume accumulations in bubble traps manually over periods of 24–72 h. At Stordalen, traps were not placed over identified points of gas bubbling, but instead

sampled overall ebullition within the area of the trap. To account for scaling effects related to the area of the traps, for these samples we report flux in terms of L gas day^{-1} m^{-2} (Table 1). In most cases we used the flux estimate for the actual sample analyzed, but in one case where a sample-specific flux estimate is not available we adopted the six-year average flux for that trap (Table 1). In all samples methane flux was calculated by multiplying the total gas flux by the measured methane concentration.

3. Results

3.1. Methane δD and δ^{13}C data

Methane δD and δ^{13}C values (Table 2) measured on the Ultra differed by variable amounts from previous measurements of the samples from Alaska and the Beaufort Sea, with an average deviation of −2 ± 9‰ for δD and −1.1 ± 0.5‰ for δ^{13}C. As discussed in Appendix 1, these differences are likely caused by interlaboratory measurement artifacts, and do not reflect changes in samples due to storage. The interlaboratory differences are minor relative to the range of variability in the samples, and do not influence the interpretations presented here. The δD values of these samples ranged from −151‰ to −383‰, and δ^{13}C values ranged from −34.3‰ to −88.8‰ (Table 2; Fig. 3). The samples from southeast Alaska, the Beaufort Sea, and two of the samples from the Alaskan North Slope (Lake Sukok, Lake Q) display relatively high δD values (>−250‰), and conform to a broad positive relationship in δD–δ^{13}C space spanning the typical ranges of thermogenic and hydrogenotrophic microbial methane (Fig. 3; note reversed *y*-axis) (Whiticar et al., 1986). In contrast, the samples from the Fairbanks area and the Stordalen Mire, as well as from Cake Eater Lake on the North Slope, display low δD values (<−250‰) and cluster in the typical δD–δ^{13}C range of fermentative microbial methane (Fig. 3). The Stordalen Mire samples display a negative trend in δD–δ^{13}C space, while most of the Fairbanks area samples display a positive trend. The low δ^{13}C (−88.8‰) and δD (−313‰) value of the sample from Killarney Lake are anomalous relative to typical values of microbial methane (Whiticar et al., 1986).
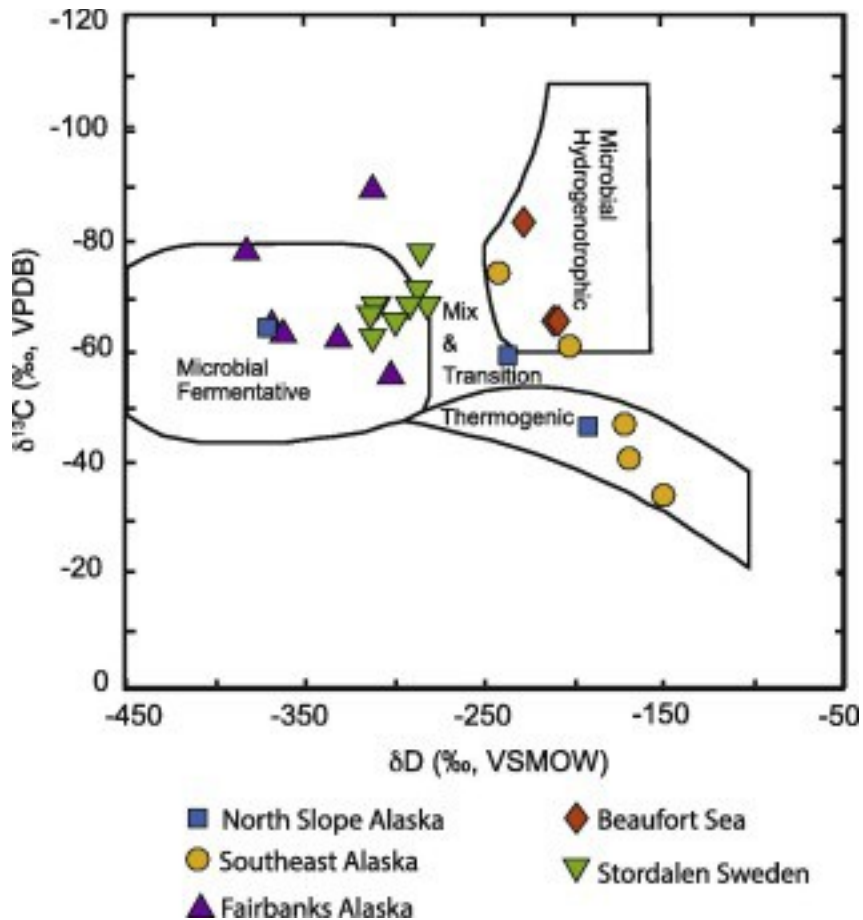
Fig. 3. Methane δD and δ¹³C values overlaid on empirical methane.
Source fields derived from Whiticar et al. (1986).

3.2. Methane clumped isotope data

The Δ_{18} values of the studied samples varied widely from −0.4‰ to +9.6‰ (Table 2, Fig. 4). For comparison, formation of methane from 0 to 100 °C in internal isotopic equilibrium would correspond to a Δ_{18} range of 7.1–4.2‰ respectively. The observed range of Δ_{18} is much wider than this, and corresponds to apparent equilibrium temperatures ranging from −61 °C to non-real temperatures (i.e., negative values of Δ_{18} do not have equivalent equilibrium temperatures). Thus both the high and low ends of the range of Δ_{18} values cannot be interpreted in the context of apparent equilibrium formation temperatures, as discussed below (Sections 4.3 Non-equilibrium microbial methane, 4.4 Mixtures of thermogenic and microbial methane, 4.5 Δ).
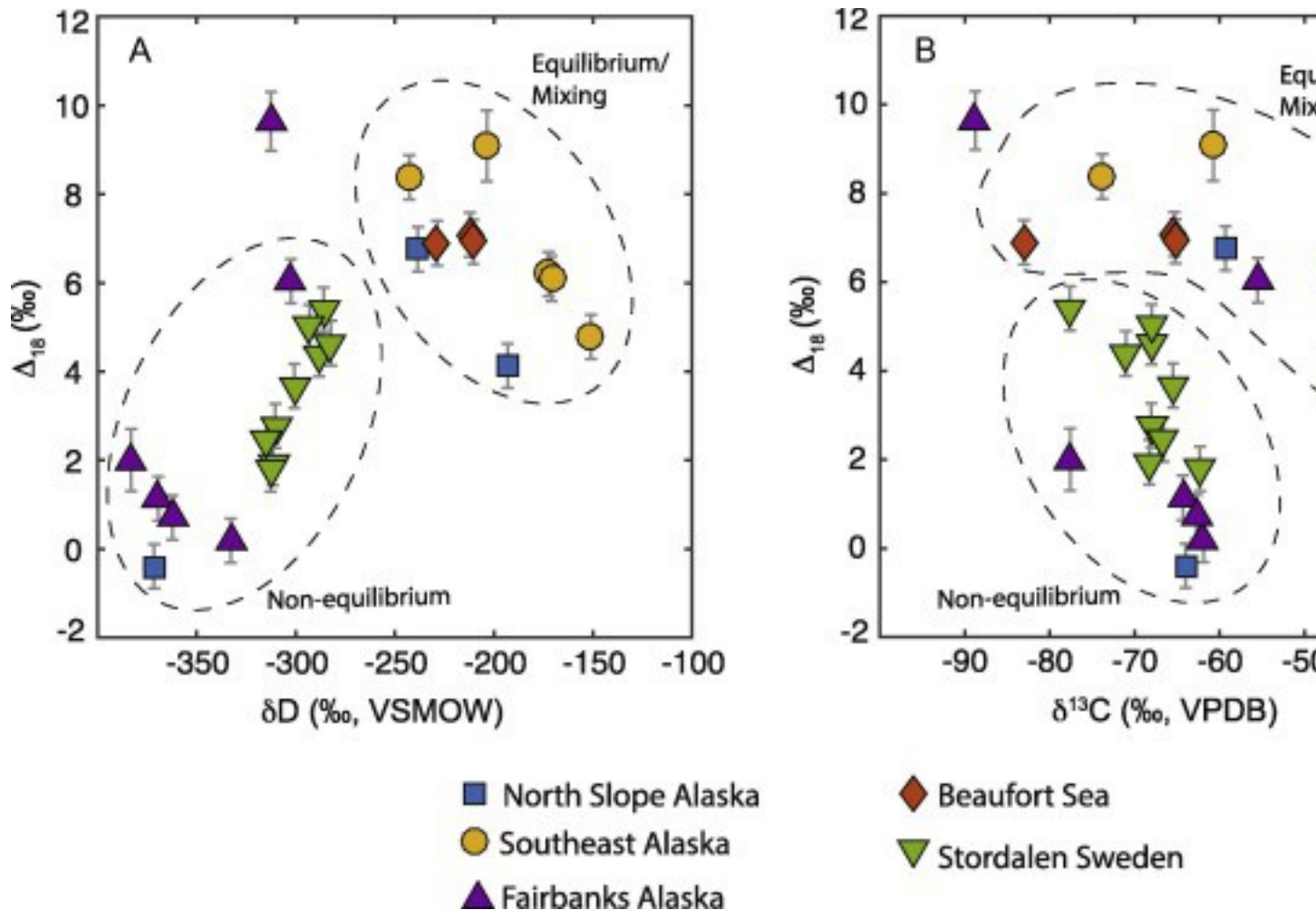
Fig. 4. Scatter plots of methane Δ_{18} versus δD (A) and $\delta^{13}C$ (B). All error bars are 2 SE as described in Section 2.5. Error bars for δD and $\delta^{13}C$ are smaller than the symbols. Two groups of data described in Section 3.2 are circled.

In specific geographic regions in Alaska we found a similarly wide range of Δ_{18} values: Δ_{18} ranged from 4.8‰ to 8.4‰ in Southeast Alaska, from 0.2‰ to 9.6‰ in the Fairbanks region, and from −0.4‰ to 6.8‰ on the North Slope. These data indicate significant differences in the origin of regional ebullitive methane emissions. The Stordalen lake samples also displayed a wide range of Δ_{18} values, from 1.8‰ to 5.4‰. In contrast, the three samples from the Beaufort Sea displayed a small range of Δ_{18} values, 6.9–7.1‰. These values correspond to a temperatures of 0–5 (±13) °C, consistent with equilibrium formation at seafloor temperatures of −1.5–1 °C (Fig. 5).
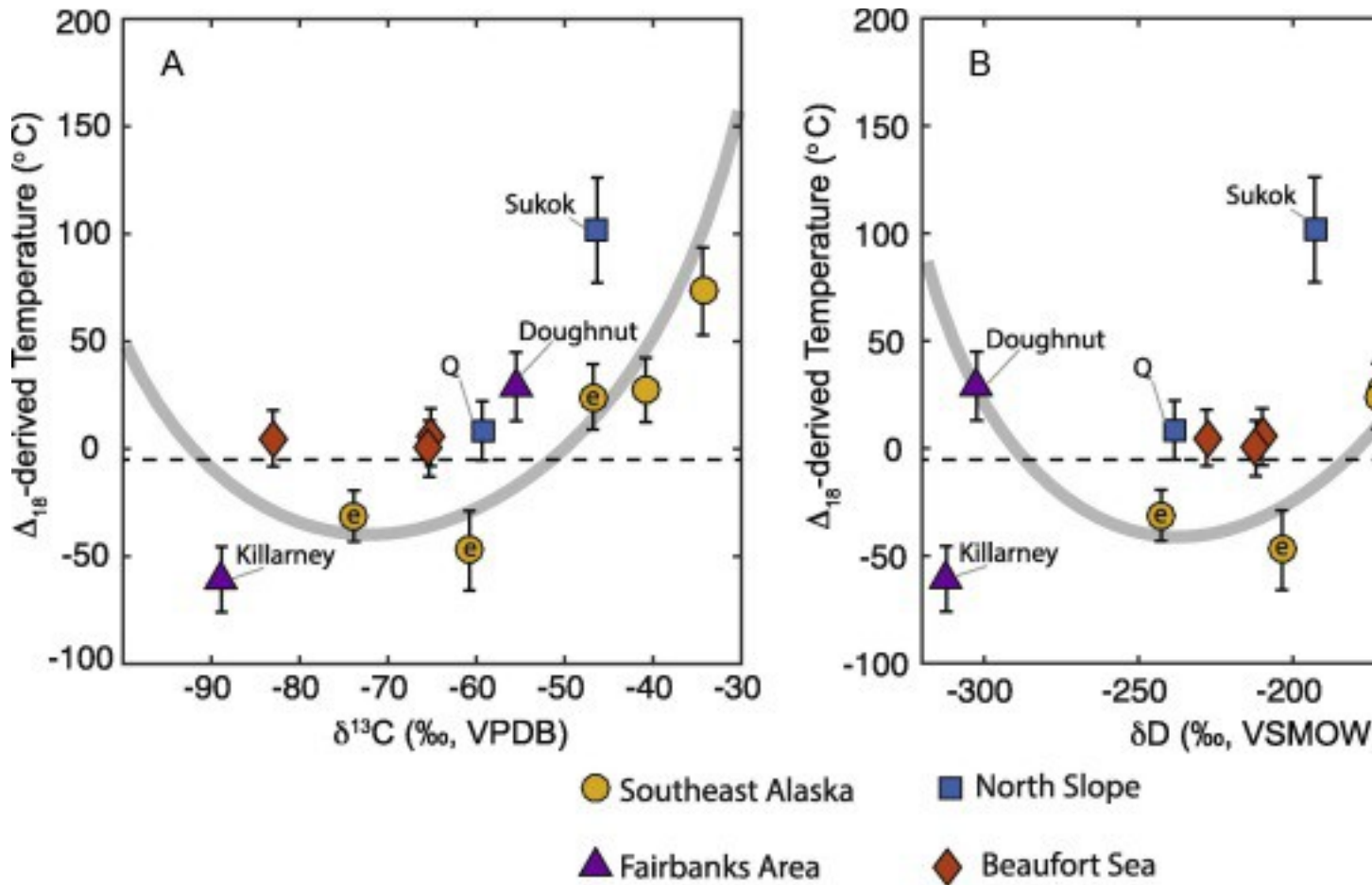
Fig. 5. Scatter plots of Δ_{18}-derived temperature versus (A) $\delta^{13}C$ and (B) δD for methane samples with inferred equilibrium or mixing-influenced Δ_{18} values. Specific samples referred to in the text are indicated. The solid gray line indicates the modeled non-linear mixing line (see Section 4.4) for samples from the Eyak Lake ("e"). The dashed line indicates a temperature of −5 °C, an assumed lower limit to methanogenesis in Arctic environments.

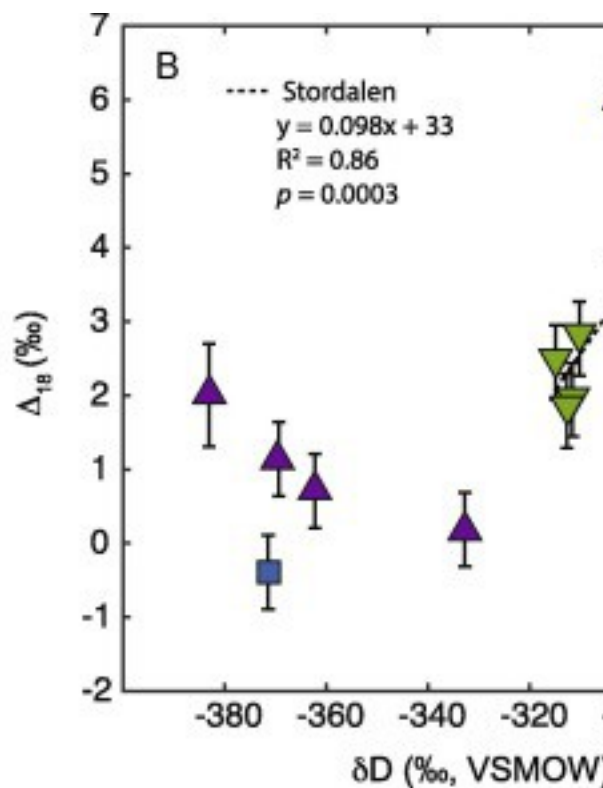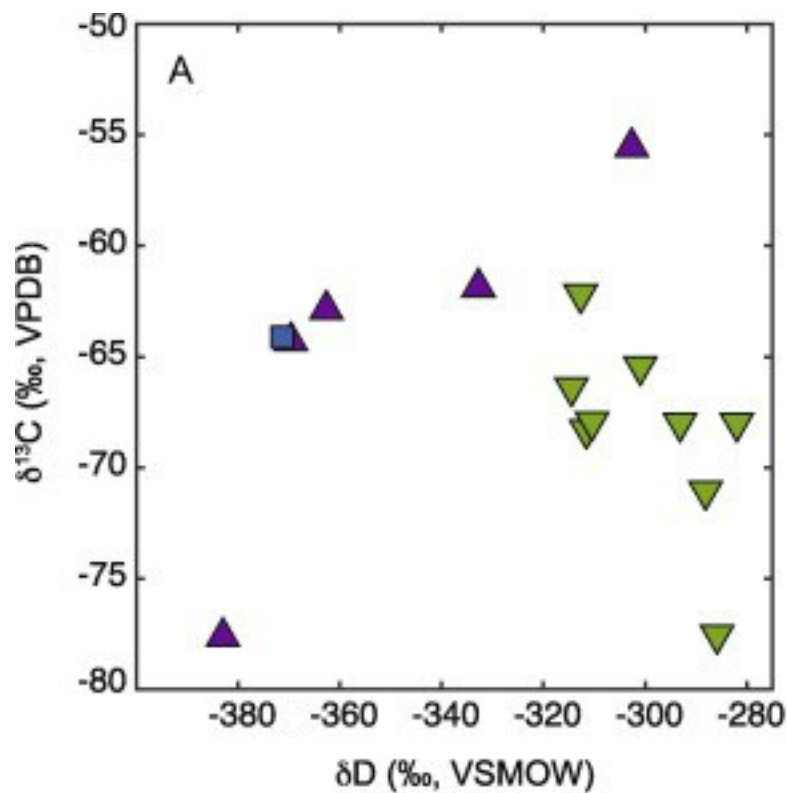The studied samples define two groups in a plot of Δ_{18} vs. δD (Fig. 4). One subset, comprising samples from southeast Alaska, the Beaufort Sea, and two of the samples from the Alaskan North Slope (Lake Sukok, Lake Q), is defined by both elevated δD values (>−250‰) and Δ_{18} values (>4‰). We interpret these samples to have either formed in isotopic equilibrium, or through mixing of isotopically distinct end-members that each formed in isotopic equilibrium (Fig. 5). The other subset, comprising the samples from the Fairbanks area and the Stordalen Mire, as well as from Cake Eater Lake on the North Slope, is defined by lower δD (<−250‰) and Δ_{18} values (<6‰) (Fig.

[4](#)). We interpret these samples to represent microbial methane that did not form in isotopic equilibrium. These Δ_{18} values, if interpreted as formation temperatures, would indicate temperatures >29 °C that are not plausible for microbial methane in Arctic [lake sediments](#). The two groups of samples are less clearly distinguished in Δ_{18}-$\delta^{13}C$ composition space ([Fig. 4](#)), but samples inferred to form in isotopic equilibrium or through mixing generally have higher $\delta^{13}C$ values, whereas samples with non-equilibrium Δ_{18} values generally have lower $\delta^{13}C$ values ([Fig. 4](#)). The Doughnut Lake sample from the Fairbanks region is ambiguous in that it plots with the equilibrium samples in $\delta^{13}C$–Δ_{18} space, but with the non-equilibrium samples in δD–Δ_{18} space. In addition, the sample from Killarney Lake (Fairbanks) is anomalous given its low δD (−312‰) and $\delta^{13}C$ (−88.8‰) values, but high Δ_{18} value (9.6‰) (see Section [4.3.1](#)).
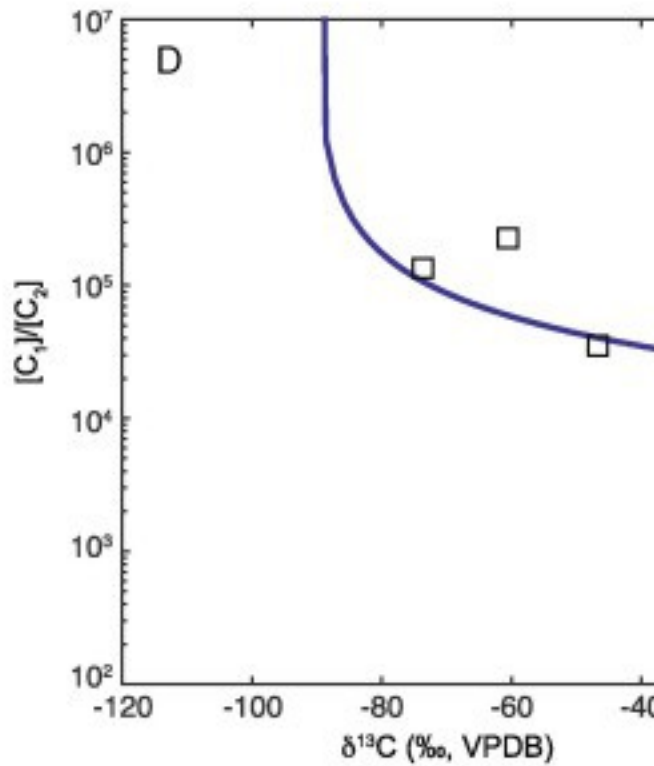
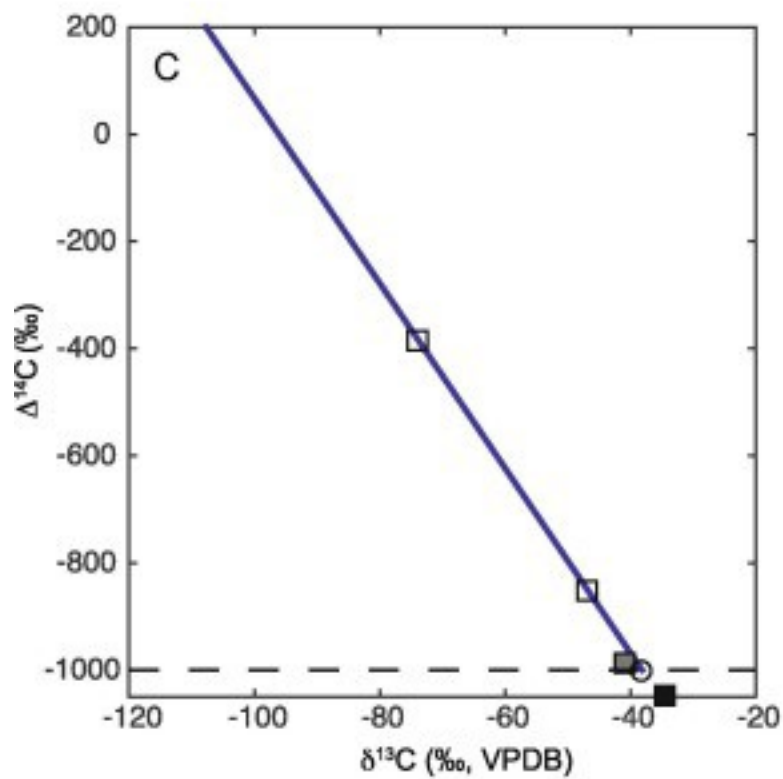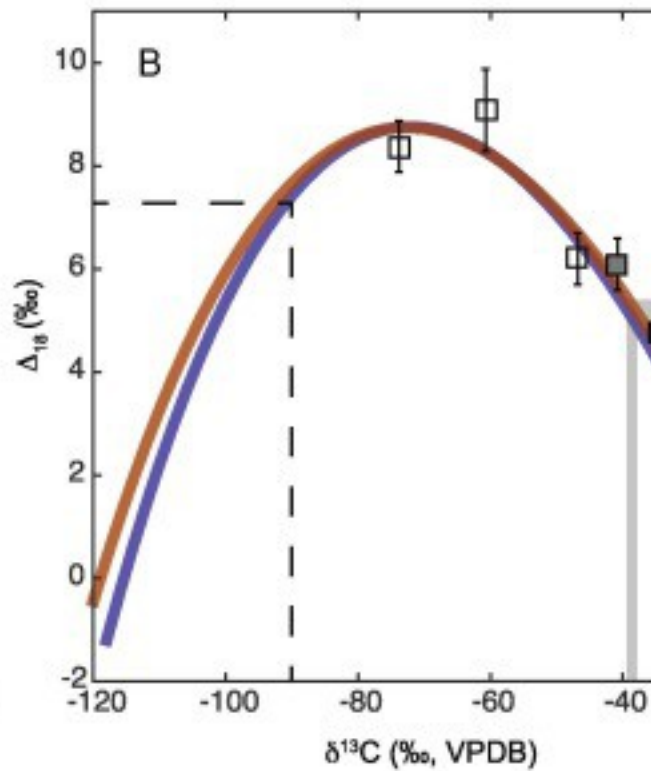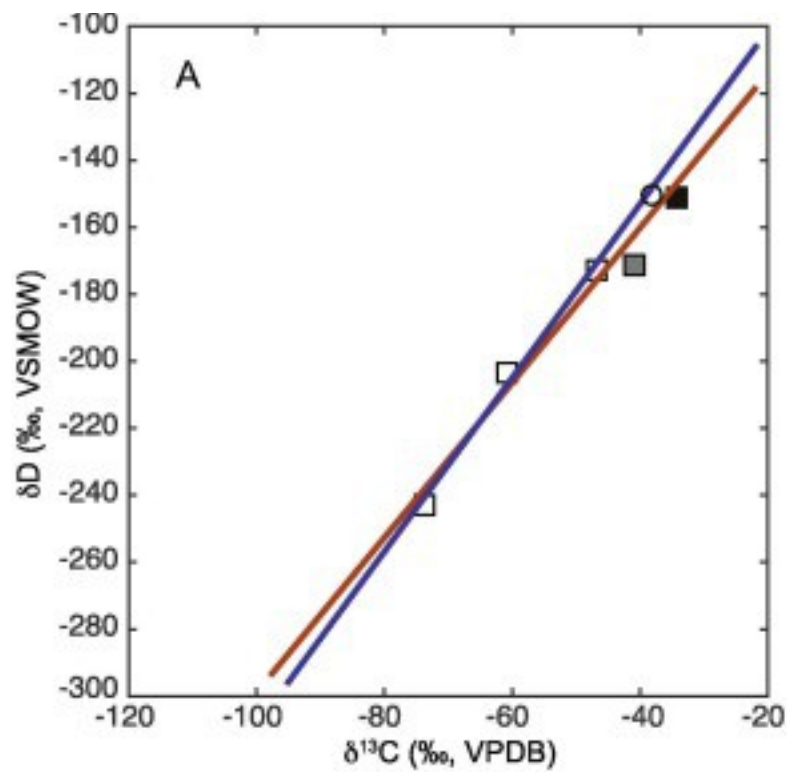3.3. Methane flux and radiocarbon data

Methane ebullitive [flux measurements](#) from lacustrine seeps in Alaska spanned eight orders of magnitude, from .005 to 93,456 L CH_4 day^{-1} trap^{-1} ([Table 1](#)). Area normalized ebullitive methane flux from the Swedish lakes spanned two orders of magnitude, from 1.5 to 183 L CH_4 day^{-1} m^{-2} ([Table 1](#)).

Methane $\Delta^{14}C$ values also spanned a substantial range ([Table 2](#); [Fig. 6](#), [Fig. 7](#)) from −265‰ (equivalent to 2420 ^{14}C years before present) to −1000‰ (no detectable radiocarbon; >50,000 ^{14}C years before present). It is important to note that methane ^{14}C ages do not necessarily indicate the age of methane formation, since in many cases recently formed methane can be produced from aged carbon that is depleted in ^{14}C (e.g. [Walter et al., 2006](#), [Walter et al., 2008](#), [Brosius et al., 2012](#)).

A

δ¹³C (‰, VPDB) vs δD (‰, VSMOW)

B

- - - - Stordalen
$y = 0.098x + 33$
$R^2 = 0.86$
$p = 0.0003$

Δ_{18} (‰) vs δD (‰, VSMOW)

C

- - - - Stordalen
$y = -0.22x - 12$
$R^2 = 0.46$
$p = 0.045$

Δ_{18} (‰) vs δ¹³C (‰, VPDB)

D

- - - - S
y
R
p

—— Alaska
$y = -26x + 35$
$R^2 = 0.85$
$p = 0.009$

Δ_{18} (‰) vs $^2\alpha_{H2O-CH4}$

E

F
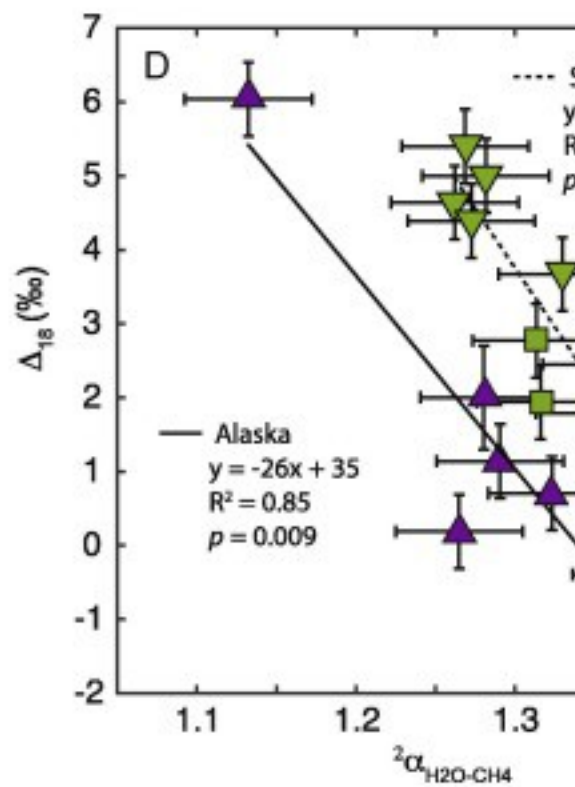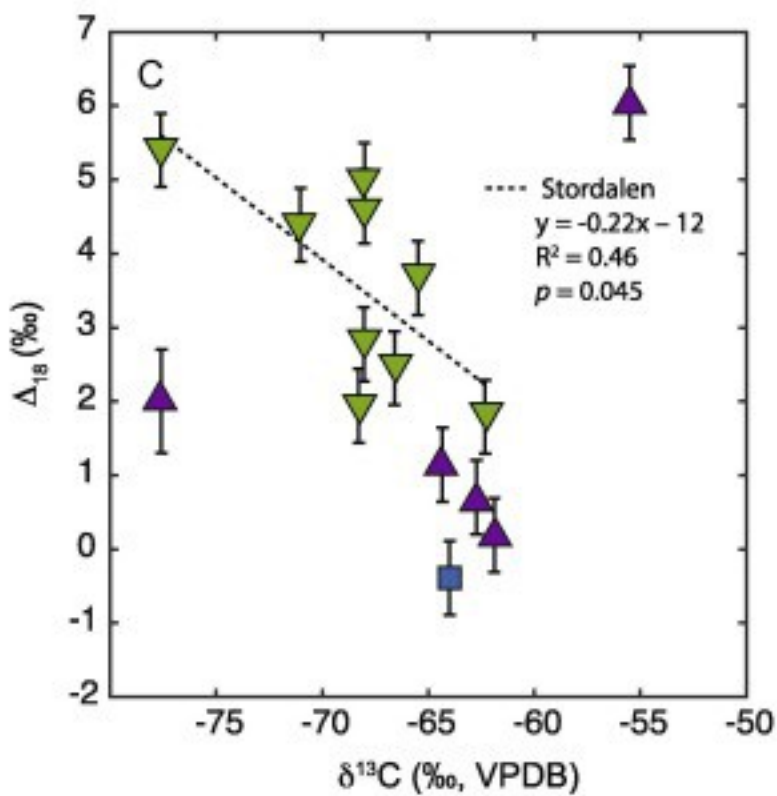
Fig. 6. Scatter plots of (A) δD vs. $δ^{13}C$; (B) δD vs. $Δ_{18}$; (C) $δ^{13}C$ vs. $Δ_{18}$; (D) $2αH2O\text{-}CH4$ vs. $Δ_{18}$ (E) $13αCO2\text{-}CH4$ vs. $Δ_{18}$; and (F) $Δ^{14}C$ vs. $Δ_{18}$ for lacustrine microbial [methane](#) samples displaying non-equilibrium $Δ_{18}$ values. Linear [regression statistics](#) for significant correlations for subsets of data either from Alaska or from the Stordalen [Mire](#) are shown; in (E) the sample from Doughnut Lake (upper right side of the plot) is an outlier and is not included in the regression model.

A

δD (‰, VSMOW)

$\delta^{13}C$ (‰, VPDB)

B

Δ_{18} (‰)

$\delta^{13}C$ (‰, VPDB)

C

$\Delta^{14}C$ (‰)

$\delta^{13}C$ (‰, VPDB)

D

$[C_1]/[C_2]$

$\delta^{13}C$ (‰, VPDB)

☐ Eyak Lake

■ Prince William Sound (PWS)

▣ Katalla

○ Estimated Eyak Lake High-Temperature End-Member

— Eyak Lake Mixing Lin...

— Eyak Lake + PWS Mix...

Fig. 7. Isotope and gas composition mixing models for methane from Eyak Lake and Prince William Sound. (A) $\delta^{13}C$ vs. δD; (B) $\delta^{13}C$ vs. Δ_{18}; (C) $\delta^{13}C$ vs. $\Delta^{14}C$; (D) $\delta^{13}C$ vs. $[C_1]/[C_2]$. The circle in (A) and (C) indicates the inferred composition of the high-temperature Eyak Lake end-member based on $\delta^{13}C-\Delta^{14}C$ and $\delta D-\Delta^{14}C$ mixing lines. The gray area in (B) indicates the high-temperature end-member Δ_{18} values implied by the $\delta^{13}C$ value (−38.1‰) inferred from the $\delta^{13}C-\Delta^{14}C$ mixing line (C). The dashed line in (B) indicates the Δ_{18} and $\delta^{13}C$ value implied by the model if the low-temperature end-member formed in equilibrium at −5 °C. Equilibrium formation at higher temperatures or non-equilibrium kinetic isotope effects would imply lower $\delta^{13}C$ values. The dashed line in (C) indicates a $\Delta^{14}C$ composition of −1000‰ (i.e. no radiocarbon). $\Delta^{14}C$ data is not available for the PWS sample and its $\delta^{13}C$ value is plotted on the *y*-axis in (C). The mixing curve in (D) is one of many possible curves that fits the data from samples Eyak-1 and Eyak-3, but is representative of the general shape of these curves. $\delta^{13}C$ and $[C_1]/[C_2]$ end-members for this curve are −90‰ and 1×10^{12} for the low-temperature end-member, and −20‰ and 25,000 for the high-temperature end-member. The Katalla sample data are plotted for reference only and are not included in the models.

3.4. Methylotrophic methanogen culture

Methane sampled from the *M. acetivorans* culture had a low δD value (−347‰), but a high $\delta^{13}C$ value (−30.2‰). The δD value of water in the culture media was −82 ± 1‰, the $\delta^{13}C$ value of the methanol was −25.69‰, and the δD value of the methyl group of methanol was −156 ± 8‰. The high $\delta^{13}C$ of the methane is likely the result of Rayleigh fractionation of the culture media methanol, and suggests that the methanogens consumed most of this carbon substrate. The Δ_{18} value for this sample, −5.4 ± 0.5‰, is the lowest yet observed. This observation suggests that cultures of fermentative methanogens produce substantial non-equilibrium effects in Δ_{18}, similar to or greater (i.e., further from equilibrium) than those observed in cultures of hydrogenotrophic methanogens (Stolper et al., 2015, Wang et al., 2015). Interpretation of this low Δ_{18} value is complicated. The Δ_{18} value of the methane is controlled by both the isotope effects associated with the hydrogenation of the methanol-derived methyl group to methane, as well as the initial isotopic order of the methyl group (Stolper et al., 2015, Wang et al., 2015). We do not know the clumped isotope composition of the methanol consumed in this experiment, which could have influenced the Δ_{18} value of the methane. Furthermore, the results of this experiment, while informative regarding Δ_{18} values in fermentative methane at a first-order, may not be

particularly representative of fermentative [methanogenesis](#) in [freshwater environments](#), for three reasons. First the cultured taxon was isolated from a [marine ecosystem](#) ([Sowers et al., 1984](#)), and was grown in a salt water medium. We used this taxon as an initial test of fermentative methanogenesis because it was readily available. Second, the carbon substrate for the culture was methanol, whereas [acetate](#) is the dominant carbon substrate for fermentative methanogenesis in most [freshwater ecosystems](#) ([Whiticar et al., 1986](#)), and differences in ^{13}C [isotopic fractionation](#) between methanogens grown with acetate and methanol on the order of 50‰ have been documented in previous studies ([Krzycki et al., 1987](#)). Third, the genera *Methanosarcina* has differences in its methanogenic pathway as compared to the genera *Methanosaeta* ([Smith and Ingram-Smith, 2007](#)), which is the dominant aceticlastic methanogen in most freshwater environments ([Borrel et al., 2011](#)). Previous studies of hydrogenotrophic methane produced by *Methanosarcina barkeri* produced lower Δ_{18} values than other hydrogenotrophic methanogens ([Stolper et al., 2015](#), [Wang et al., 2015](#)). Therefore the metabolic pathway of *Methanosarcina* could produce more pronounced non-equilibrium effects in Δ_{18} than that of other methanogens.

4. Discussion

Based on the Δ_{18}, δD, and $\delta^{13}C$ values summarized above, supplemented in some cases with $\Delta^{14}C$ values and ratios of [methane](#) to [ethane](#) concentrations ($[C_1]/[C_2]$), we divided the studied samples into four categories of methane sources: thermogenic methane, equilibrium microbial methane, non-equilibrium microbial methane, and mixtures of methane from deep and shallow sources. The basis for this categorization is discussed below. We primarily interpret Δ_{18} values as an indicator of equilibrium or non-equilibrium isotope [fractionation](#) at the time of methane formation, although we do discuss post-formation [isotope effects](#) related to mixing and [gas-phase](#) diffusion in Sections [4.3.1 High Δ](#), [4.4 Mixtures of thermogenic and microbial methane](#). A key limitation of our interpretation is that we do not have constraints on how methane oxidation influences Δ_{18} values. Previous research has suggested, however, that methane oxidation does not strongly influence the [isotopic composition](#) of methane bubbles emitted from lakes ([Walter et al., 2008](#)).

4.1. Thermogenic methane

The methane sampled from Lake Sukok on the North Slope of Alaska displayed a Δ_{18} value of 4.1 ± 0.5‰, corresponding to an apparent equilibrium temperature of 102 ± 24 °C. This inferred temperature is within the range at which thermogenic

methane typically forms (~60 to ~300 °C), and would imply generation of gas during initial catagenic breakdown of organic macromolecules to oil and gas (Hunt, 1979, Quigley and Mackenzie, 1988, Clayton, 1991, Seewald, 2003). We note that Δ_{18} data for other thermogenic methane samples have yielded temperatures >140 °C (Stolper et al., 2014b, Wang et al., 2015), except for dominantly thermogenic gases from the Antrim Shale (95–115 °C) (Stolper et al., 2015). The elevated δD (−193‰) and δ^{13}C values (−46.3‰), low Δ^{14}C value (−998‰) of the Lake Sukok sample are also consistent with a thermogenic origin. Furthermore, Walter Anthony et al. (2012)showed that the hydrocarbon geochemistry and isotopes of the Sukok Lake ebullition seep closely matched data from an adjacent petroleum production well. A recent study of pore water geochemistry and geobiology from Lake Sukok also concluded that most or all of the methane found in its sediments is thermogenic in origin, and that there is very little methanogenactivity in Lake Sukok sediments based on the abundance of both genetic markers and lipid biomarkers (Matheus Carnevali et al., 2015).

4.2. Equilibrium microbial methane

We interpret the clumped isotope data from the three Beaufort Sea samples, as well as the sample from Lake Q in Alaska, to be indicative of microbial methane generated in internal isotopic equilibrium. There are three lines of evidence for this conclusion. First, the Δ_{18} values for these samples (6.8–7.1‰) imply formation temperatures between 0–9 ± 13 °C (Fig. 5), which is within error of ambient environmental temperatures, and well below the lower limit of thermogenic methane formation (~60 °C; Hunt, 1979, Seewald, 2003). Second, the δD (−210‰ to −238‰) and δ^{13}C (−59.3‰ to −83‰) values of all four gases are within the typical range of microbial methane (Table 2; Fig. 3; (Whiticar et al., 1986). Third, research to date indicates that microbial methane formed in marine and deep subsurface settings, produces equilibrium clumped isotope signatures that reflect their formation environment (Stolper et al., 2014b, Stolper et al., 2015, Inagaki et al., 2015, Wang et al., 2015).

4.2.1. Microbial methane from the Beaufort shelf and slope

The three methane samples from the Beaufort Sea slope and shelf vents and sediment core indicate consistently low formation temperatures, from 0 to 5 (±13) °C. These temperatures are within error of bottom water temperatures at these sites (−1.5–1 °C; Paull et al., 2011, Paull et al., 2015). The Δ_{18} data are consistent with methane formation in sediments or sub-permafrost environments, and do not support a dominant contribution from thermogenic methane or deep microbial methane formed in warm

environments (>18 °C). Overall, our results from the Beaufort shelf are consistent with previous clumped-isotope analyses of marine methane seeps from the Santa Barbara Basin and the Santa Monica Basin, which indicated formation temperatures (6–16 °C), within error of bottom water temperatures (Stolper et al., 2015). Similarly, analyses of gas hydrate and sediment core void gas from the North Cascadia Margin indicated relatively low formation temperatures between 12 and 42 °C (Wang et al., 2015). The Beaufort Sea samples exhibit similar Δ_{18} values in spite of large differences in water depth and vent type. The 38 m water depth methane vent is inferred to be a pingo-like formation associated with melting permafrost (Paull et al., 2007, Paull et al., 2011). This sample contains negligible radiocarbon (−997‰ $\Delta^{14}C$; Table 2), in contrast to nearby sedimentary organic matter that contains more radiocarbon (−960 to −831‰ $\Delta^{14}C$; Paull et al., 2011). This difference in $\Delta^{14}C$ between methane and sedimentary organic matter is probably caused by the migration of methane from deeper subsurface horizons that contain ancient carbon, possibly as a result of dissociating gas-hydrates or permafrost (Paull et al., 2007, Paull et al., 2011). The Δ_{18} data are consistent with this interpretation, but argue against a high-temperature origin for methane from gas hydrates. Permafrost extends up to 700 m below the seafloor in this area (Paull et al., 2011), and it is possible that methane could be forming in relatively deep sub-permafrost environments that maintain temperatures near 0 °C.

The 420 m vent on the Beaufort Shelf is classified as a mud volcano, and is not associated with permafrost (Paull et al., 2015). The isotopic and ionic chemistry of water venting from the volcano suggest a contribution of fluid derived from smectiteto illite clay dehydration (Paull et al., 2015), which is thought to occur at temperatures of ∼60 °C or greater (Jennings and Thompson, 1986), although the water chemistry also implies a contribution from seawater and groundwater of meteoric origin to the fluid emanating from the mud volcano (Paull et al., 2015). Our clumped isotope data rule out a high formation temperature for the methane at this mud volcano, and instead imply microbial methanogenesis in sediments or the shallow subsurface. Methane sampled from a nearby sediment core is similar in its Δ_{18}, $\delta^{13}C$, and δD values (Table 2), further suggesting a shallow source for the mud volcano methane. It is possible that the methane was originally formed in the shallow subsurface, was subsequently buried to a greater depth where clay dehydration took place, and then both the methane and clay-dehydration waters were exhumed to form the modern mud volcano. Heating of buried methane to temperatures around 60 °C would most likely have not reset its Δ_{18} value, as a previous study implied that internal isotopic re-equilibration does not occur at this temperature (Stolper et al., 2014b).

4.2.2. Deep subsurface microbial methane emitted from Alaskan lakes

We interpret the clumped-isotope measurement from one of the Alaskan lakes, Lake Q, to indicate emission of subsurface microbial methane formed in internal isotopic equilibrium. Methane emitted at Lake Q has a Δ_{18} value of 6.8 ± 0.5‰, equivalent to a formation temperature of 9 ± 13 °C (Fig. 5). This inferred temperature is within error (2 SE) of the estimated mean annual temperature at the lake (~0 °C). The methane from this seep, however, contains no detectable radiocarbon (Table 2), arguing against microbial methanogenesis in lake sediments. In addition, as discussed in detail below (Sections 4.3 Non-equilibrium microbial methane, 4.5 Δ), all samples of microbial methane produced in freshwater sediments analyzed to date have displayed low, non-equilibrium Δ_{18} values (Stolper et al., 2015, Wang et al., 2015). We infer that the low temperatures of methane generation, combined with the lack of radiocarbon, are consistent with methane emitted from Lake Q being produced by methanogens consuming fossil carbon in coal seams known to underlie the lake (Walter Anthony et al., 2012). Microbial coal-bed methane has been documented in other regions of Alaska (Dawson et al., 2012), and is an important category of coal-bed methane globally (Strąpoć et al., 2011). Furthermore, a recent study found evidence for methane formed in clumped-isotope equilibrium at ~70 °C in a coaldeposit in deep marine sediments (Inagaki et al., 2015).

Methane from Doughnut Lake has a Δ_{18} value of 6.0‰, indicating an apparent temperature of 29 ± 15 °C (Fig. 5). This result is ambiguous, as it could reflect either equilibrium methane formation by deep subsurface methanogens, or methane formation in lake sediments with a relatively small non-equilibrium isotope effect (Fig. 6; Section 4.3). Given this ambiguity we include the Doughnut Lake sample in our discussion of non-equilibrium microbial methane below.

4.3. Non-equilibrium microbial methane

Six of the methane samples from lakes in Alaska (Goldstream-Hotspot, Goldstream-Tinies, Goldstream-40A, Smith, Cake Eater, and Doughnut), and all of the Stordalen samples, have δD (−285‰ to −383‰) and δ¹³C (−55.5‰ to −77.6‰) values (Fig. 6A) typical of microbial methane, but low Δ_{18} values (6‰ to −0.4‰) (Table 2, Fig. 6B and C). These Δ_{18} values would require implausible temperatures for methanogenesis in lake sediments (29–905 °C; negative Δ_{18} values do not correspond to any temperature) if interpreted as equilibrium values (Table 2), and almost certainly do not reflect formation of methane in internal isotopic equilibrium. Instead, the low Δ_{18} values for these samples are consistent with previous studies that showed microbial methane produced in

freshwater sediments, cow rumen, and in pure cultures of hydrogenotrophic methanogens have low Δ_{18} values that are not in equilibrium with their formation environment (Stolper et al., 2014a, Stolper et al., 2015, Wang et al., 2015). Previous studies have proposed that non-equilibrium Δ_{18} values in microbial methane primarily represent kinetic isotope effects related to the differential reversibility of the enzymatic reactions involved in methanogenesis (Stolper et al., 2015, Wang et al., 2015). In other words, this hypothesis proposes that kinetic isotope effects manifest in Δ_{18} values, as well as in δD and $\delta^{13}C$ values, are determined by the extent to which the reactions of methanogenesis operate near thermodynamicreversibility, which controls the establishment of isotopic equilibration between methane and its metabolic precursors (Blair, 1998, Valentine et al., 2004, Penning et al., 2005). The 'reversibility of methanogenesis' is related to chemical potential gradients between methane and its precursors. Faster rates of methanogenesis at high chemical potential gradients are interpreted to correlate with less reversible reactions, larger kinetic isotope effects, and lower Δ_{18} values (Valentine et al., 2004, Penning et al., 2005, Stolper et al., 2015, Wang et al., 2015). Other factors in addition to the rate of methanogenesis, including differences in metabolic pathways between methanogen taxa, the relative abundance of methanogenesis reactants and products in the environment, and the allocation of carbon for growth as opposed to methane generation, could also be influential in the reversibility of methanogenesis and related isotope effects (Valentine et al., 2004, Stolper et al., 2015, Wang et al., 2015).

In the context of this hypothesis, we propose two explanations for the substantial variability of Δ_{18} values observed in the microbial methane from the Alaskan and Swedish lakes. First, it could indicate differences in the extent of kinetic fractionation exhibited by methanogenesis between samples. This would imply that the highest Δ_{18} value (Doughnut Lake; 6‰) corresponds to a high degree of reversibility, and the lowest Δ_{18}value (Cake Eater Lake; −0.4‰) corresponds to low reversibility. Alternatively, the range in Δ_{18} values could represent variable mixtures of two distinct sources of microbial methane. For example, mixing of microbial methane formed in isotopic equilibrium, possibly in deep subsurface environments, with non-equilibrium methane formed in lake sediments, would produce methane samples with intermediate non-equilibrium Δ_{18} values. In this scenario, the non-linearity of mixing would be minimized if the δD and $\delta^{13}C$ values of the end-members were similar (Fig. 1). A strong positive correlation between δD and Δ_{18} in the Stordalen Mire samples (Fig. 6B; $R^2 = 0.86$) is suggestive of a mixing relationship between isotopically distinct methane reservoirs. However, correlations between $\delta^{13}C$ and Δ_{18} (Fig. 6C; $R^2 = 0.46$), and between δD and

$\delta^{13}C$ (Fig. 6A; R^2 = 0.37), are weaker for this group of samples, suggesting that if such mixing occurred, it was modulated by other isotopic effects. We also note that there are no currently known sources of deep subsurface microbial methane in the Fairbanks area or in the Stordalen Mire complex.

Previous studies (Stolper et al., 2015, Wang et al., 2015) have noted a negative correlation between non-equilibrium Δ_{18} and $2\alpha H2O\text{-}CH4$ values, an association that is consistent with the hypothesis that microbial methane isotope fractionation is controlled by the reversibility of methanogenesis (Valentine et al., 2004). We also observe a negative correlation between Δ_{18} and $2\alpha H2O\text{-}CH4$ in the non-equilibrium methane samples (R^2 = 0.34), although there is substantial scatter in this relationship (Fig. 6D). If the data are subdivided into the Alaskan and Stordalen samples, however, the correlation between Δ_{18} and $2\alpha H2O\text{-}CH4$ for each sample set is much stronger (Fig. 6D, R^2 = 0.85 and 0.72, respectively). The different regression lines for these two sample groups could be caused by differences in the source of water δD data. Namely, for the Alaskan samples we applied δD measurements of permafrost ice, but for the Stordalen samples we applied measurements of lake water. Overall, the negative correlations between Δ_{18} and $2\alpha H2O\text{-}CH4$ values are consistent with the hypothesis that the degree of reversibility during methanogenesis at least partially controls Δ_{18} in the studied lakes.

We also observe a positive correlation between Δ_{18} and $13\alpha CO2\text{-}CH4$ values (Fig. 7E) in five samples from Alaskan lakes (Fig. 6C; R^2 = 0.77); the sample from Doughnut Lake does not conform and is not included in the regression model. This relationship could also indicate kinetic isotope effects that influence both Δ_{18} and $13\alpha CO2\text{-}CH4$ (Valentine et al., 2004, Penning et al., 2005, Stolper et al., 2015), similar to the relationship between Δ_{18} and $2\alpha H2O\text{-}CH4$ described above. Indeed, such a relationship is predicted by a model of kinetic isotope effects in methane, described in Stolper et al. (2015). While we do not have CO_2 isotope data for the Stordalen lake samples, these samples display a negative relationship between methane $\delta^{13}C$ and Δ_{18} (Fig. 6C) that would be consistent with the pattern observed in the Alaskan lakes if $CO_2 \delta^{13}C$ values are relatively constant in these samples.

Among the Alaskan lake methane samples, those with low $\Delta^{14}C$ (<−970‰) display higher Δ_{18} values than samples with high $\Delta^{14}C$ (>−400‰) (Fig. 6F; note that we do not have $\Delta^{14}C$ data for the Goldstream-Tinies sample). This pattern could indicate a greater degree of reversibility in methanogenesis sustained by older, more refractory carbon that is inherently more difficult to degrade, which would limit rates of methanogenesis. Alternatively, this pattern could be explained by variable mixtures of ^{14}C-depleted

methane, formed in isotopic equilibrium in the deep subsurface, with relatively ^{14}C-enriched methane that is formed out of isotopic equilibrium in lake sediments.

The wide range of Δ_{18} values in the microbial lacustrine methane samples indicates that kinetic isotope effects associated with methanogenesis vary substantially in the studied Arctic lakes. Invariably there is some degree of mixing of methane in lake sediments, but our results are not consistent with simple mixing between an equilibrium end-member and a non-equilibrium end-member with a constant Δ_{18} value. Instead the observed trends, and in particular relationships between Δ_{18} and $2\alpha H2O$-CH4 and $13\alpha CO2$-CH4 values ([Fig. 6]D and E), are consistent with methane being produced in these lakes with a variety of non-equilibrium Δ_{18} values, which would imply a spectrum of kinetic isotope effects.

4.3.1. High Δ_{18} in microbial methane from Lake Killarney

The methane sampled from Lake Killarney has an unexpectedly high Δ_{18} value of 9.6 ± 0.7‰ (2 SE of two replicate measurements), which corresponds to an equilibrium formation temperature of −61 ± 15 °C. This temperature is clearly unrealistic for methanogenesis ([Fig. 5]), and the anomalously high Δ_{18} value is in the opposite direction of previously observed non-equilibrium effects ([Stolper et al., 2014b], [Stolper et al., 2015], [Wang et al., 2015]), which produce lower Δ_{18} values than expected for a given temperature. Currently, we cannot account for this result, but we suggest three possible explanations. First, this high Δ_{18} value could reflect mixing of thermogenic and microbial methane ([Fig. 1]). However, the highly depleted $\delta^{13}C$ value of this sample (−88.8‰) makes such mixing seem unlikely, as it would require that the microbial end-member have an even lower $\delta^{13}C$ value, which would be anomalous for microbial methane in [freshwater environments]([Fig. 3]).

Second, the high Δ_{18} value could be the result of methane oxidation, whose effects on Δ_{18} values have not yet been directly observed. However, methane oxidation tends to cause enrichment of residual methane in both δD and $\delta^{13}C$ ([Whiticar, 1999]), and – given the especially low $\delta^{13}C$ signature of this sample – it is unlikely that it has undergone significant oxidation. Third, the high Δ_{18} value could be the result of diffusive [isotopic fractionation]. The effects of gas-phase diffusion on clumped isotope compositions have been described in detail for mass-47 CO_2 and mass-4 H_2 by [Eiler and Schauble (2004)] and [Eiler (2013)], respectively. In brief, diffusive isotopic fractionation of methane in air would be expected to lower both δD and $\delta^{13}C$ values in the diffused gas by approximately 14‰, but increase Δ_{18} values by approximately 1.5‰. While this effect will require empirical validation, and does not take into account the likely importance of [liquid-phase]diffusion in this environment, to a first-order it is consistent with the high

Δ_{18} and low δD and $\delta^{13}C$ values observed at Killarney Lake. It is currently unclear why diffusion would impart a significant effect on methane emitted at Killarney Lake and not the other sites in this study, with the possible exception of Eyak Lake as discussed below.

4.4. Mixtures of thermogenic and microbial methane

The isotopic compositions of the five samples from Southeast Alaska (Eyak-1, -2, and -3; PWS; Katalla) suggest that they contain variable mixtures of methane from high- and low-temperature formation environments. Such mixing was previously identified for a larger set of methane samples from Lake Eyak and Prince William Sound by Walter Anthony et al. (2012) on the basis of evidence for linear correlations between $\Delta^{14}C$, $\delta^{13}C$ and δD values. That study suggested that the mixing end-member with high $\delta^{13}C$ and δD values, and a low $\Delta^{14}C$ value, was thermogenic in origin.

The Δ_{18} values for the Lake Eyak and Prince William Sound (PWS) samples in this study are consistent with mixing between methane with distinct δD and $\delta^{13}C$ values. These samples form a parabolic trajectory in $\delta^{13}C$–Δ_{18} and δD–Δ_{18} space (Fig. 7B) that is characteristic of mixtures in which the end-member δD and $\delta^{13}C$ values differ widely (Fig. 1). The Δ_{18} value for sample PWS indicates a formation temperature of 73 ± 20 °C (Table 2; Fig. 5), which is a plausible, but low, temperature for thermogenic methane formation (Hunt, 1979, Seewald, 2003). In contrast, sample Eyak-1 indicates a temperature of 24 ± 15 °C, which is too low for a thermogenic source, and samples Eyak-2 and Eyak-3 indicate temperatures of −47 ± 19 and −31 ± 12 °C respectively (Table 2), which are implausible for methane formation by any mechanism in these environments (Fig. 5). The high Δ_{18} values and low corresponding apparent temperatures for the Lake Eyak samples can be understood, however, as a consequence of mixing between thermogenic and microbial methane that differ in their Δ_{18}, $\delta^{13}C$ and δD values.

We calculated a best-fit mixing model (described in detail in Appendix 3) to the Δ_{18}, $\delta^{13}C$ and δD values from the Lake Eyak and PWS samples. As discussed below, there is some evidence that the PWS sample does not conform to the same mixing trend as the Lake Eyak samples, and therefore we calculated a second model that omits this sample (Fig. 7A and B). While the two models differ slightly, qualitatively the results are similar. A key assumption of these mixing models is that mixing is conservative and involves only two-end members. The mixing models provide a good fit (within 0.5‰ in Δ_{18}) to samples Eyak-1, Eyak-3, and PWS, but a less good fit (within 0.8‰ in Δ_{18}) to sample Eyak-2 (Fig. 7B), although this difference is within the 2 SE analytical error of this

sample. The mixing models constrain the possible combinations of Δ_{18}, $\delta^{13}C$ and δD values for the mixing end-members, but not their specific values.

Specifically, the models suggest that in order for the low-temperature end-member to have an equilibrium formation temperature above −5 °C, it would require that its $\delta^{13}C$ value be less than −90‰ ([Fig. 7]B), which is anomalously low compared to other samples from [freshwater ecosystems] ([Whiticar, 1999]). As discussed above, microbial methane in most lakes expresses non-equilibrium Δ_{18} values lower than that equivalent to their formation temperature, but in this case a low non-equilibrium Δ_{18} value would require a $\delta^{13}C$ value even lower than −90‰. Alternatively, the Lake Eyak low-temperature end-member may be characterized by a higher than equilibrium Δ_{18} value, as observed at Killarney Lake, which could be caused by diffusion or another undetermined post-formation process.

Additional measurements, including radiocarbon and [gas composition] data, provide further constraints on gas mixing at Eyak Lake. If we assume that the $\Delta^{14}C$ value of the high-temperature end-member is −1000‰ (i.e. it contains no radiocarbon), the $\delta^{13}C$ of the high-temperature end-member can be constrained by the intersection of a $\Delta^{14}C$ value of −1000‰ and the $\Delta^{14}C$–$\delta^{13}C$ mixing line for samples Eyak-1 and Eyak-3 ([Fig. 7]C). This constraint implies a high-temperature end member $\delta^{13}C$ value of −38.1 ± 1‰, although this estimate is based on only two radiocarbon measurements, which limits its accuracy. This inferred high-temperature end-member $\delta^{13}C$ value is lower than the $\delta^{13}C$ value for sample PWS (−34.3‰) ([Fig. 7]C). This difference suggests that either (1) the high-temperature methane emitted at Eyak Lake differs in $\delta^{13}C$ from the high-temperature methane emitted in the PWS sample, despite their close proximity (see Fig. 6 in [Walter Anthony et al., 2012]); or (2) that the first assumption is invalid and there are more than two low-temperature end-members with distinct $\Delta^{14}C$ values; or (3) that sample PWS underwent post-formation isotopic fractionation, such as oxidation, that led to a higher $\delta^{13}C$ value.

If the $\delta^{13}C$ (−38.1‰) value for the high-temperature end-member inferred from the $\Delta^{14}C$ mixing-line discussed above is correct, this in turn implies that the Δ_{18} of the thermogenic end-member is approximately 5.2 ± 0.5‰ ([Fig. 7]B), indicating a temperature of 57 ± 19 °C. This is an anomalously low temperature for thermogenic methane generation, suggesting an extremely low maturity source ([Seewald, 2003]), despite the relatively high $\delta^{13}C$ value. One possible explanation is that the high-temperature end-member is not thermogenic in origin, and instead is deep surface microbial methane. Comparing our results with [C$_1$]/[C$_2$] data for the Lake Eyak samples indicates further complexity in the gas mixing relationships in this region. While sample Eyak-2 is

intermediate in δD and $δ^{13}C$ values, it has the highest $[C_1]/[C_2]$ value (Fig. 7D). This implies that the assumption of conservative, two end-member mixing is incorrect, and suggests that either (1) there are more than two mixing end-members or (2) that ethane oxidation is occurring and disproportionately affected sample Eyak-2. Furthermore, the relatively high $[C_1]/[C_2]$ value for sample Eyak-1 implies that the high-temperature end-member has a $[C_1]/[C_2]$ ratio greater than 1×10^4 (Fig. 7D), which is anomalously high for thermogenic methane (Bernard et al., 1978, Whiticar, 1999). These data also suggest that the high-temperature end-member is likely microbial methane, potentially produced in coal beds that occur in Southeast Alaska (Dawson et al., 2012, Walter Anthony et al., 2012).

Ultimately, the high $Δ_{18}$ values of methane in the vicinity of Lake Eyak confirm that mixing between isotopically distinct end-members is occurring, and has the potential to provide new insights into the formation environment of the mixing end-members. However, comparison with gas composition data suggests that the mixing processes occurring in this system are more complex than can be adequately resolved within the scope of this paper.

Methane sampled from Katalla, ~80 km to the east of Lake Eyak, has a similar isotopic signature to sample Eyak-1 (Fig. 7A and B). The Katalla methane δD and $δ^{13}C$ values plot within the thermogenic methane field (Table 2, Fig. 3), but the inferred clumped-isotope temperature of 27 ± 15 °C is not consistent with pure thermogenic methane (Fig. 5). Furthermore, the Katalla sample contains no detectable ethane. This suggests that the methane emitted at Katalla is predominantly microbial in origin, and either represents a mixture of high- and low-temperature microbial methane with distinct δD and $δ^{13}C$ values, or methane with a single source forming around 27 °C with highly enriched δD and $δ^{13}C$ values. The relatively low $δ^{13}C$ value of CO_2 in the Katalla sample (−37.9‰, Table 1) also suggests that this sample may have undergone methane oxidation (Whiticar, 1999).

4.5. $Δ_{18}$ variability in microbial methane

We compared our dataset for microbial methane emissions from the Arctic and for the methylotrophic methanogen culture experiment with existing clumped-isotope data for microbial methane (Stolper et al., 2015, Wang et al., 2015). Fig. 8 depicts deviations in 2αH2O-CH4 and $Δ_{18}$ (or $Δ_{13CH3D}$) relative to their equilibrium values at the estimated temperature of methane formation, following Stolper et al. (2015), and were calculated as follows:

$$(10) \quad \Delta\Delta18 = \frac{18R18R*m}{18R18R*e} - 1 \times 1000$$

$$(11) \quad \Delta2\alpha H2O\text{-}CH4 = \frac{2\alpha H2O\text{-}CH4,m}{2\alpha H2O\text{-}CH4,e} - 1 \times 1000$$
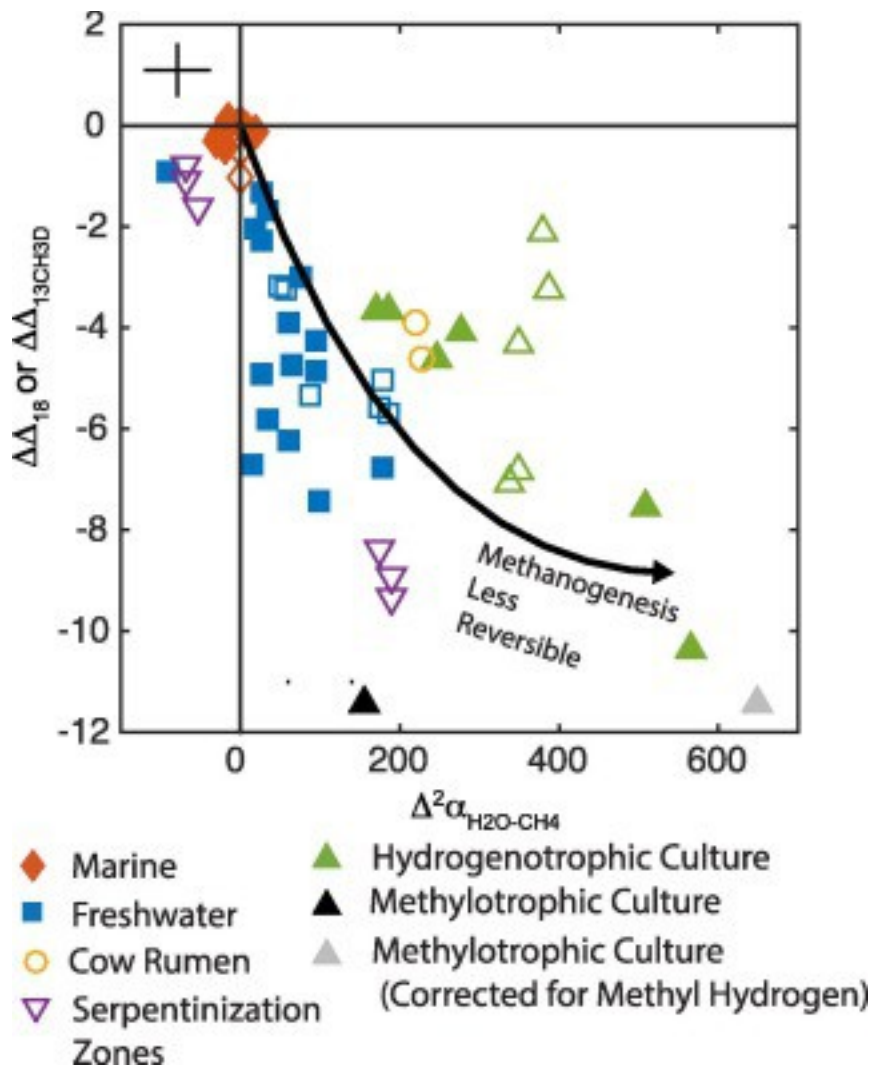
Fig. 8. Compilation of microbial methane Δ_{18} and Δ_{13CH3D} data, comparing the deviation in measured Δ_{18} or Δ_{13CH3D} values relative to the expected value if the methane formed in internal isotopic equilibrium vs. the deviation in measured $2\alpha_{H2O-CH4}$ relative to the value expected in heterogeneous phase isotopic equilibrium (for definitions of axis parameters see Eqs. (1), (1)). Data are from this study, Stolper et al. (2015), and Wang et al. (2015). Data from Wang et al. (2015) (open points) were measured as Δ_{13CH3D}. The solid line indicates values predicted by a model of the isotopic composition of methane formed by hydrogenotrophic methanogens as a function of the reversibility of methyl-coenzyme M reductase (Stolper et al., 2015), with reversibility decreasing away from the origin. The gray triangle represents the $2\alpha_{H2O-CH4}$ value for the water-derived hydrogen atoms in the methylotrophic culture sample under two assumptions: (a) 50% of methane hydrogen atoms are derived from water; and (b) there is no D/H fractionation between methyl

group hydrogen and methane. Representative *x* and *y* error bars are indicated in the upper left corner.

Equilibrium values for $^{18}R/^{18}R*$ and 2αH2O-CH4 were based on the [temperature dependence](#) of Δ_{18} and 2αH2O-CH4 presented by [Stolper et al., 2014a](#), [Stolper et al., 2015](#), respectively. Measurements performed at the Massachusetts Institute of Technology (MIT) by [Wang et al. (2015)](#) (unfilled symbols in [Fig. 9](#)) were reported as $\Delta^{13}CH_3D$, as these measurements were made using a spectroscopic method that only measures the abundance of $^{13}CH_3D$ ([Ono et al., 2014](#)). $^{12}CH_2D_2$ is assumed to have a minor influence on Δ_{18} values in most natural samples ([Stolper et al., 2014b](#)), and our analysis treats deviations from equilibrium Δ_{13CH3D} and Δ_{18} values as comparable at the scale of variability depicted here. $\Delta\Delta_{13CH3D}$values were calculated as in Eq. [(10)](#), but substituting $^{13CH3D}R/^{13CH3D}R*$ for $^{18}R/^{18}R*$. Equilibrium values for $^{13CH3D}R/^{13CH3D}R*$ were derived from the calculations of [Webb and Miller (2014)](#). Water δD data for culture samples were not presented in [Wang et al. (2015)](#), so we assumed a value of −50‰ as an estimate for laboratory water at MIT ([Bowen et al., 2007](#)).
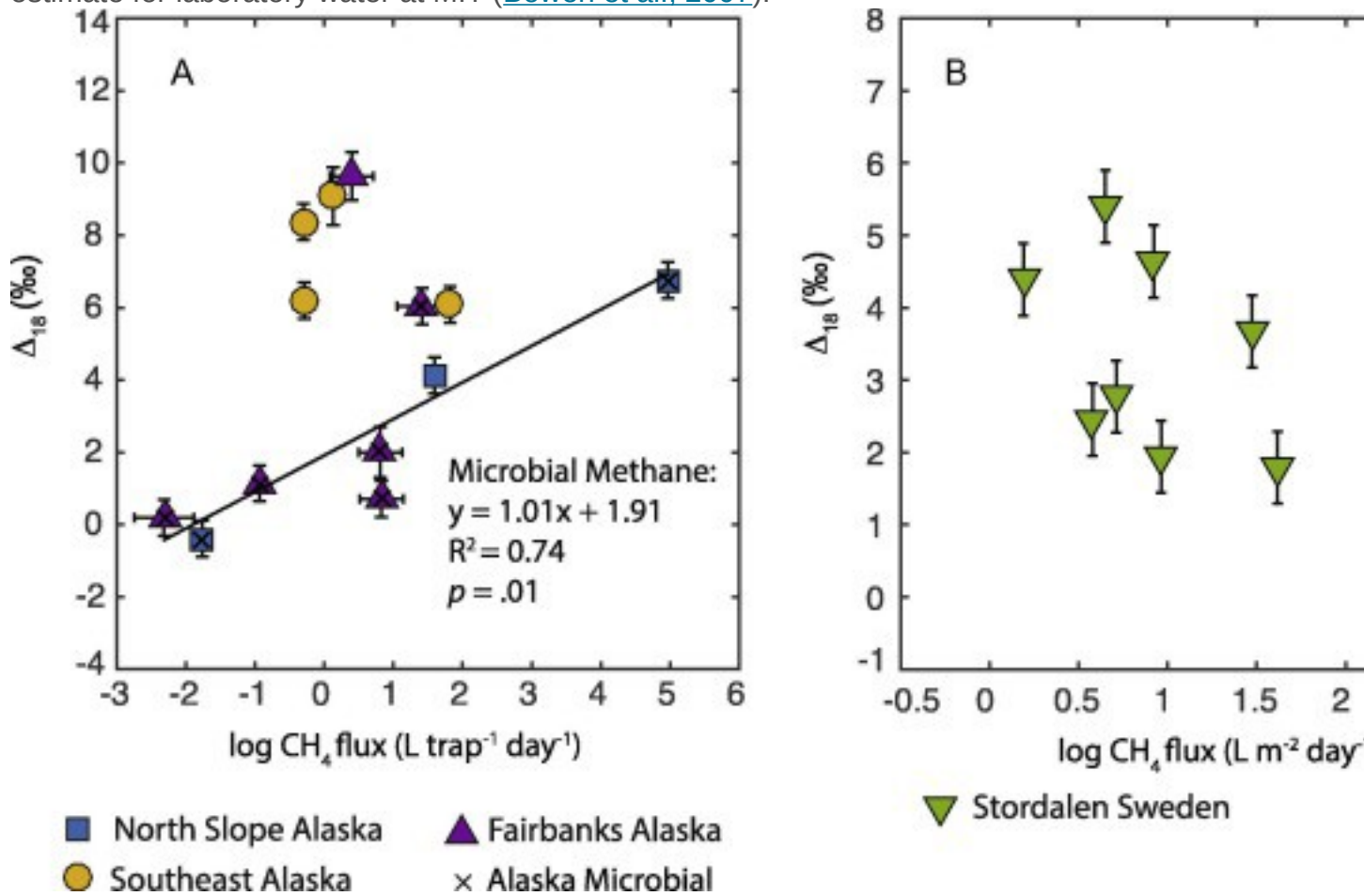
1. [Download high-res image (249KB)](#)

Fig. 9. Scatter plot of log CH_4 flux vs. Δ_{18} for (A) Alaskan lacustrine seep samples and (B) Stordalen lake samples. The Alaskan samples were collected at localized methane seeps and their fluxes are calculated on a per trap basis. The Stordalen samples were not collected at specific sites of methane seepage, and their flux is normalized to the area of the trap. A positive linear regression fit for microbial methane samples from Alaska (excluding samples where mixing or diffusion effects have likely altered primary Δ_{18} values) is shown in (A).

Several key patterns emerge from this compilation. First, all marine samples cluster near the defined equilibrium values, while all other sample categories show variability in Δ_{18} and 2αH2O-CH4, with values that deviate substantially from equilibrium (Fig. 8). This difference has been noted previously (Stolper et al., 2015, Wang et al., 2015), and may be related to either slower rates of methanogenesis in marine environments, or to anaerobic oxidation reactions causing the isotopic equilibration of methane, as suggested for the equilibration of $\delta^{13}C$ values (Yoshinaga et al., 2014, Stolper et al., 2015).

Second, the methylotrophic methanogen culture analyzed in this study is clearly distinct from previous hydrogenotrophic methanogen cultures, in that it exhibits much lower Δ2αH2O-CH4values relative to its departure from equilibrium Δ_{18}. This difference could be related to different sources of hydrogen, since fermentative methanogenesis is thought to derive ∼75–50% of its hydrogen atoms from methyl groups of substrate molecules (Pine and Barker, 1956, Schoell, 1980, Sugimoto and Wada, 1995, de Graaf et al., 1996, Waldron et al., 1999, Chanton et al., 2006), whereas hydrogenotrophic methane derives its hydrogen atoms either from water or from H_2 that is assumed to be in isotopic equilibrium with water (Daniels et al., 1980, Schoell, 1980, Balabane et al., 1987, Sugimoto and Wada, 1995, Valentine et al., 2004).

If we assume that 50% of the hydrogen in the fermentative culture methane is derived from the substrate methanol, and that there is no isotopic fractionation between methanol and methane, by mass balance the 2αH2O-CH4 value for the remaining two methane hydrogen atoms is 2.01. Plotting this value in Fig. 8 (with a gray triangle) brings the methylotrophic culture much closer to the data from the hydrogenotrophic methanogen experiments. Assuming that 75% of the hydrogen atoms are from the substrate methanol results in a much larger 2αH2O-CH4 value of 13.5 (not plotted because it does not fit on the scale of Fig. 8). This calculation depends on the assumption that there is no hydrogen isotope fractionation between methyl group substrates and methane. We are aware of one isotopic labeling study that suggests

minimal hydrogen isotope fractionation between [acetate](#) and methane during fermentative methanogenesis ([Pine and Barker, 1956](#)). We note however, that differences between the aceticlastic and methylotrophic pathways could lead to larger hydrogen isotope fractionations in methyl hydrogen from methanol. While not well constrained, this calculation suggests that it is possible that the differences in $\Delta 2\alpha H2O\text{-}CH4\text{–}\Delta\Delta_{18}$ space between the hydrogenotrophic and methylotrophic methanogen cultures could be a result of their differing hydrogen sources.

Alternatively, kinetic isotope effects for both $2\alpha H2O\text{-}CH4$ and Δ_{18} could differ between different pathways of methanogenesis. Such differences could be caused by differences in kinetic isotope effects associated with the [enzymes](#) used by different methanogenesis pathways, and may be especially important with respect to the distinctive metabolism of the genus *Methanosarcina* ([Smith and Ingram-Smith, 2007](#)). Furthermore, relatively lower Δ_{18} values in fermentative methane could be caused by an inherited kinetic clumped isotope signature in the methyl group of the substrate molecule (i.e. acetate or methanol) ([Wang et al., 2015](#)). Whatever its cause, the difference in trajectories followed in a plot of $\Delta 2\alpha H2O\text{-}CH4$ vs. $\Delta\Delta_{18}$ potentially provides a means of distinguishing fermentative and hydrogenotrophic methane.

Third, the hydrogenotrophic culture samples are also clearly distinct from freshwater methane samples ([Fig. 8](#)). This suggests that non-equilibrium isotope fractionation in freshwater methanogenesis follows a trajectory in $\Delta 2\alpha H2O\text{-}CH4\text{–}\Delta\Delta_{18}$ space that is distinct from that of the studied hydrogenotrophic methanogen cultures. Comparison with the methylotrophic culture suggests that the trajectory in freshwater methane may be related, at least in part, to fermentative methanogenesis, which is inferred to be dominant in many freshwater ecosystems ([Whiticar et al., 1986](#), [Whiticar, 1999](#)). As discussed above, this trajectory may be in part controlled by differences in the hydrogen source between hydrogenotrophic and fermentative methanogens.

Fourth, a model of kinetic isotope effects in methanogenesis, described in detail in [Stolper et al. (2015)](#), fits some of these data ([Fig. 9](#)B), and predicts the general trend observed. There are, however, also clear deviations from the model prediction. For example, some hydrogenotrophic culture samples exhibit higher $\Delta\Delta_{18}$ values and lower $\Delta 2\alpha H2O\text{-}CH4$ values than the model prediction. In contrast, some freshwater and [serpentinization](#) samples, as well as the fermentative culture sample, exhibit lower $\Delta\Delta_{18}$ values and higher $\Delta 2\alpha H2O\text{-}CH4$ values than the model prediction. These discrepancies are almost certainly related to the simplicity of the model, which assumes a single kinetic isotope effect in methanogenesis during [hydrogenation](#) of a methyl group to generate methane by methyl-coenzyme M reductase. Increased model

complexity, through the addition of kinetic isotope effects at other reaction steps, could potentially accommodate this complexity, but is beyond the scope of this paper. Additionally, differences in the fractional contribution of hydrogen atoms from water, differential kinetic isotope effects of enzymes in different pathways of methanogenesis, or inherited non-equilibrium clumped isotope values from methyl substrates could influence the expression of Δ_{18} and 2αH2O-CH4 values in fermentative microbial methane and contribute to deviations from the model prediction.

4.6. Implications for natural Arctic methane emissions

Understanding the future responses of methane emissions in the Arctic is an important component of predicting carbon cyclefeedbacks to anthropogenic greenhouse warming (Schuur et al., 2008, O'Connor et al., 2010, Koven et al., 2011). The data presented in this study demonstrate that clumped-isotope analyses can help to distinguish microbial and thermogenic methane, can differentiate between different sources of microbial methane (i.e. deep vs. shallow methanogens), can identify mixtures of methane with different origins, and can provide new insights into the properties of those mixtures. Temporal monitoring of Δ_{18} values, in tandem with other isotopic measurements, could prove especially valuable in understanding how the relative flux of different methane sources vary with changing environmental conditions.

The clumped-isotope data presented in this study confirms the presence of diverse sources of methane in lakes from three regions of Alaska. On the North Slope, thermogenic methane, coal-bed microbial methane, and lake sediment microbial methane are emitted from seeps within 100 km of one another. In Southeastern Alaska, the studied seeps emit variable mixtures of methane from high- and low-temperature formation environments. Our results are consistent with the finding of Walter Anthony et al. (2012) that some ebullitive seeps in Alaskan lakes emit methane from deep subsurface reservoirs of either thermogenic or microbial origin. Comparing Δ_{18} results with methane flux estimates makes clear that some seeps associated with deep subsurface reservoirs emit methane at significantly higher flux than the bubble fluxes of microbial methane produced in lake sediments (Fig. 9). While this does not constrain the relative fluxes of these different methane sources to the atmosphere, it does highlight that deep subsurface methane reservoirs can contribute to large point sources of natural methane emissions. The Δ_{18} of methane samples from the Beaufort Shelf and Slope are consistent with formation in low temperature shallow environments, and imply that high temperature methane reservoirs need not be invoked to explain high-flux methane point sources in the Arctic Ocean.

Arguably the most important methane-related feedbacks to global warming will be associated with microbial methane emissions from wetlands, lakes, and other surficial aquatic environments (O'Connor et al., 2010, Fisher et al., 2011). Our understanding of non-equilibrium Δ_{18} signatures in microbial methane is currently incomplete, but the available data are consistent with the hypothesis that the reversibility of methanogenesis influences Δ_{18} values. In the Fairbanks, North Slope and Stordalen Mire lakes the large variability in Δ_{18} values suggest a wide range of kinetic isotope effects associated with methanogenesis (Fig. 7), as well as possible isotope effects related to methane diffusion or oxidation leading to high Δ_{18} values at Killarney Lake. Future studies of pure cultures and natural methane samples will further illuminate the controls on non-equilibrium Δ_{18} values, and this measurement could become a useful indicator of methanogenesis biochemistry and its response to environmental change.

In seeps emitting microbial methane from Alaska, excluding samples from Southeast Alaska and Killarney Lake where mixing or diffusion probably cause elevated Δ_{18} values, we observe a positive correlation between methane flux and Δ_{18} (Fig. 9A). We suggest that within this sample set, stronger kinetic isotope effects during microbial methanogenesis, which cause lower non-equilibrium Δ_{18} values, are associated with lower fluxes. One possible explanation for this association relates to differences in the source and transport mechanism for different categories of methane seeps. Walter et al. (2008) hypothesized that high-flux 'hot-spot' seeps in thermokarst lakes that exhibited older ^{14}C ages represented conduits that integrated methane production across a relatively large volume of deep, Pleistocene-aged sediments. In contrast, lower-flux seeps with younger ^{14}C ages emitted methane produced in a relatively small volume of shallow sediments.

The Δ_{18} data suggests that methane being emitted from high-flux seeps is produced with reduced kinetic isotope effects, possibly indicating slower rates of growth in deeper environments with limited substrate availability. This pattern is also consistent with the observation of higher Δ_{18} values in methane with older ^{14}C ages (Fig. 7F). If this is the case, it would imply that the high fluxes of methane from these 'hot-spot' seeps is primarily controlled by the large source volume of methane producing sediments, despite relatively slow kinetics of methanogenesis. We do not observe a correlation between flux and Δ_{18} in microbial methane from the Stordalen lake samples. This suggests that in these glacial lakes in discontinuous permafrost, where there are not clearly defined methane seeps, there is no apparent relationship between methane flux and the kinetics of methanogenesis.

5. Conclusions

We have presented a survey of the clumped isotope composition of methane emissions from Arctic environments, alongside measurements of δD, $\delta^{13}C$, and $\Delta^{14}C$. Our analysis of methane from lake ebullition seeps in Alaska indicates a diverse set of origins, including thermogenic methane, mixed microbial and thermogenic methane, microbial methane formed in isotopic equilibrium in marine and coal-bed environments, and microbial methane produced in lake sediments exhibiting non-equilibrium clumped isotope effects. Our results confirm that some lacustrine seeps emit methane formed in deep subsurface environments at temperatures ranging from 9 ± 14 to 102 ± 23 °C. Δ_{18} values from seeps on the Beaufort Shelf indicate low formation temperatures consistent with methane formation in sediments or sub-permafrost environments. While Δ_{18} values of coal-bed and marine microbial methane indicate plausible equilibrium formation temperatures, microbial methane produced in lake sediments in Alaska and Sweden are characterized by low Δ_{18} values indicating non-equilibrium isotope effects. Mixing between isotopically-distinct methane sources produces a distinctive non-linear trajectory in Δ_{18} values that can be used to help characterize the mixing end-members.

Comparison of Δ_{18} and 2αH2O-CH4 data from microbial methane produced in lake sediments supports the hypothesis that non-equilibrium Δ_{18} values are controlled, at least in part, by kinetic isotope effects related to the reversibility of methanogenesis. Both methane analyses from these lakes and a pure culture of a methylotrophic methanogen, however, follow a trajectory in 2αH2O-CH4–Δ_{18} space that differs from that for cultures of hydrogenotrophic methanogens, which could either reflect differential effects of methanogenesis pathway on Δ_{18} values, or differences in apparent hydrogen isotope fractionation related to the source of methane hydrogen. We observe a wide range of non-equilibrium Δ_{18} values in ebullitive methane fluxes, spanning a range of about 5‰, implying that kinetic isotope effects during methanogenesis are highly variable in lacustrine environments.

Acknowledgments

discussions on the results of the culture experiment. The development of the Ultra was funded by NSF-EAR, and PMJD was supported in part by Royal Dutch Shell.

Appendix 1: Interlaborotory comparison of methane δD and δ¹³C data

Aliquots of the methane samples from the Alaskan lakes and Beaufort Sea were previously analyzed for δD and δ¹³C using a gas chromatography-isotope ratio mass spectrometry method at either Florida State University, the University of Alaska, or Isotech Laboratories (Paull et al., 2011, Paull et al., 2015, Brosius et al., 2012, Walter Anthony et al., 2012). The δD and δ¹³C values measured using the Ultra are typically depleted in δD and δ¹³C relative to the previous measurements, with an average deviation of −2 ± 8‰ for δD and −1.1 ± 0.5‰ for δ¹³C (Fig. A1). We ascribe this difference to interlaboratory measurement artifacts. The Ultra measurements are anchored to off-line combustion and water reduction techniques, coupled with dual inlet mass spectrometry, performed in the laboratories of A. Schimmelmann at Indiana University (Stolper et al., 2014a). The techniques used in most conventional stable isotope laboratories have other bases for standardization, and the methane isotope community as a whole is currently organizing a broader interlaboratory approach to standardization. Thus, we do not believe we can currently resolve these discrepancies in our study, but they should be resolvable in the near future. In any event, these differences do not affect the interpretation of the results presented here. As all of our measurements are internally referenced to the same standard, issues of inaccuracy in δD or δ¹³C of a few per mil make no difference to the Δ_{18} measurements beyond the stated error of the measurement. The lower δD and δ¹³C values measured by the Ultra are not consistent with gas-phasediffusion-related fractionation caused by leakage of gas during storage, which would lead to both the δD and δ¹³C values of residual methane being higher by the same amount (Criss, 1999). Additionally, oxidation during storage should have led to increases in δD and δ¹³C as well, although by different amounts (Whiticar, 1999).
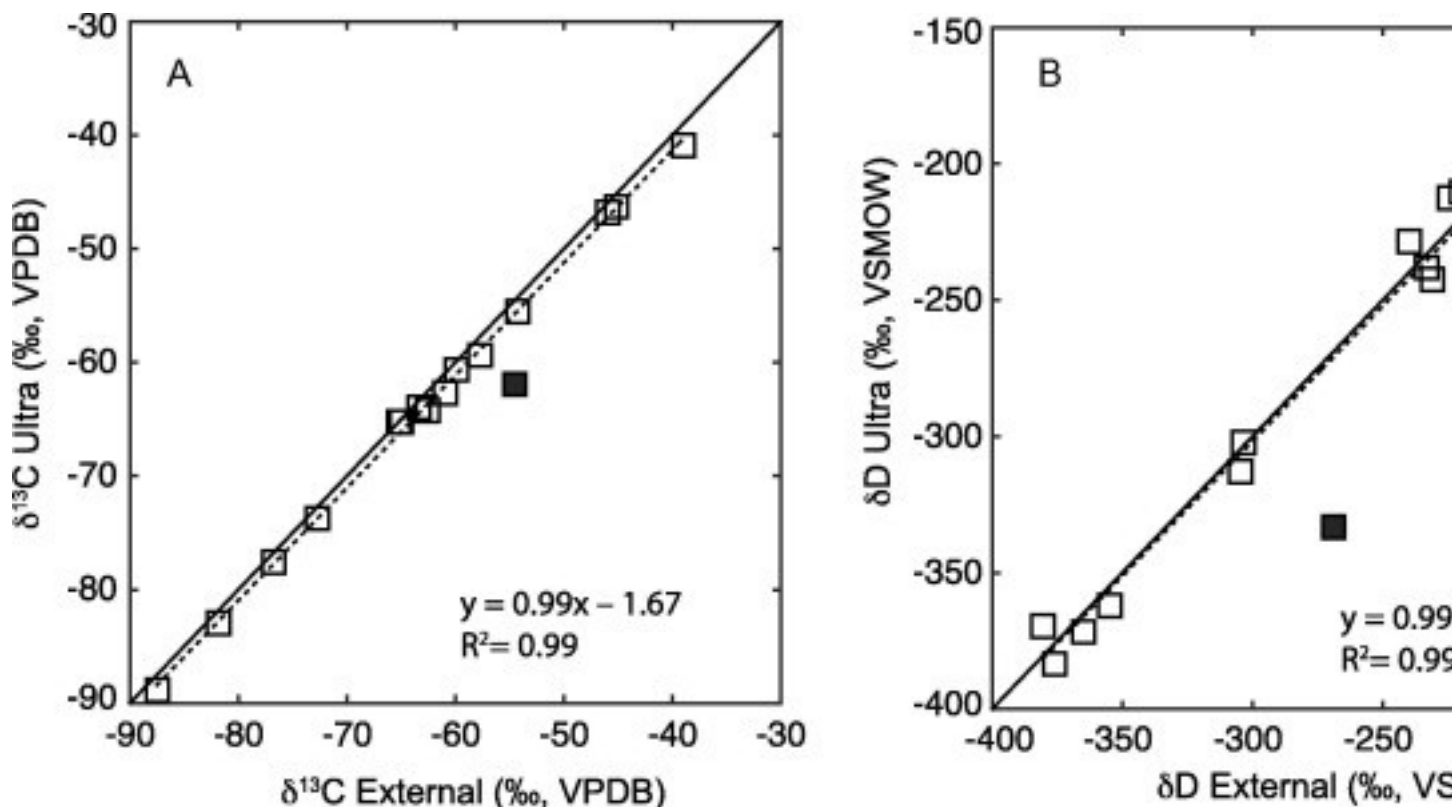
Fig. A1. Comparison of $\delta^{13}C$ (A) and δD (B) values for samples in this study measured on the Ultra and in external laboratories. The solid black line indicates a 1:1 relationship, and the dashed line indicates the linear regression fit for the data. One outlier sample (Goldstream 40A) is indicated by a filled symbol, and is not included in the linear regression fit.

For one sample (Goldstream 40A) we observe much larger deviations between the previously measured isotope values (difference of −64‰ in δD and −7.3‰ in $\delta^{13}C$). While we are uncertain of the cause of this discrepancy, we proceed with an interpretation of this sample based on the stable isotope measurements made using the Ultra (with the simple reasoning that at least we know these values apply directly to the aliquot of gas for which Δ_{18} was measured).

Appendix 2: Standardization and error estimates for clumped isotope measurements

In each session we measured [methane](#) with different [isotopic compositions](#) equilibrated on a nickel catalyst at 500 °C to determine whether Δ_{18} values were dependent on average molecular methane isotopic composition. These methane samples ranged from

−78‰ to −340‰ in δD, from −34‰ to −42‰ in δ¹³C, and from 121‰ to −198‰ in δ^{18}.
δ^{18} is defined as:

(A1) $\delta 18 = 18R_{sample}/18R_{standard} - 1$

and is expressed in per mil (‰) notation. The standard for δ^{18} values is the laboratory internal methane standard, which has a defined value of 0‰ (see Section 2.5). In previous studies, it was demonstrated that there was not a significant dependence of Δ_{18} values on the bulk isotopic composition of the gases (Stolper et al., 2014a, Stolper et al., 2014b, Stolper et al., 2015). However, in some of the measurement periods for this study a linear dependence of Δ_{18} on the bulk composition of the sample (indicated by δ^{18} values) was apparent (Fig. A2). In particular in the final measurement period, in which a total of 10 heated gas measurements were made, the linear dependence of Δ_{18} on δ^{18} was consistent throughout the session (Fig. A2A). In this session we also tested the observed dependence by measuring gases heated at 200 °C, in which we observed a linear relationship between Δ_{18} on δ^{18} with the same slope as the relationship for the gases heated at 500 °C (Fig. A2A).
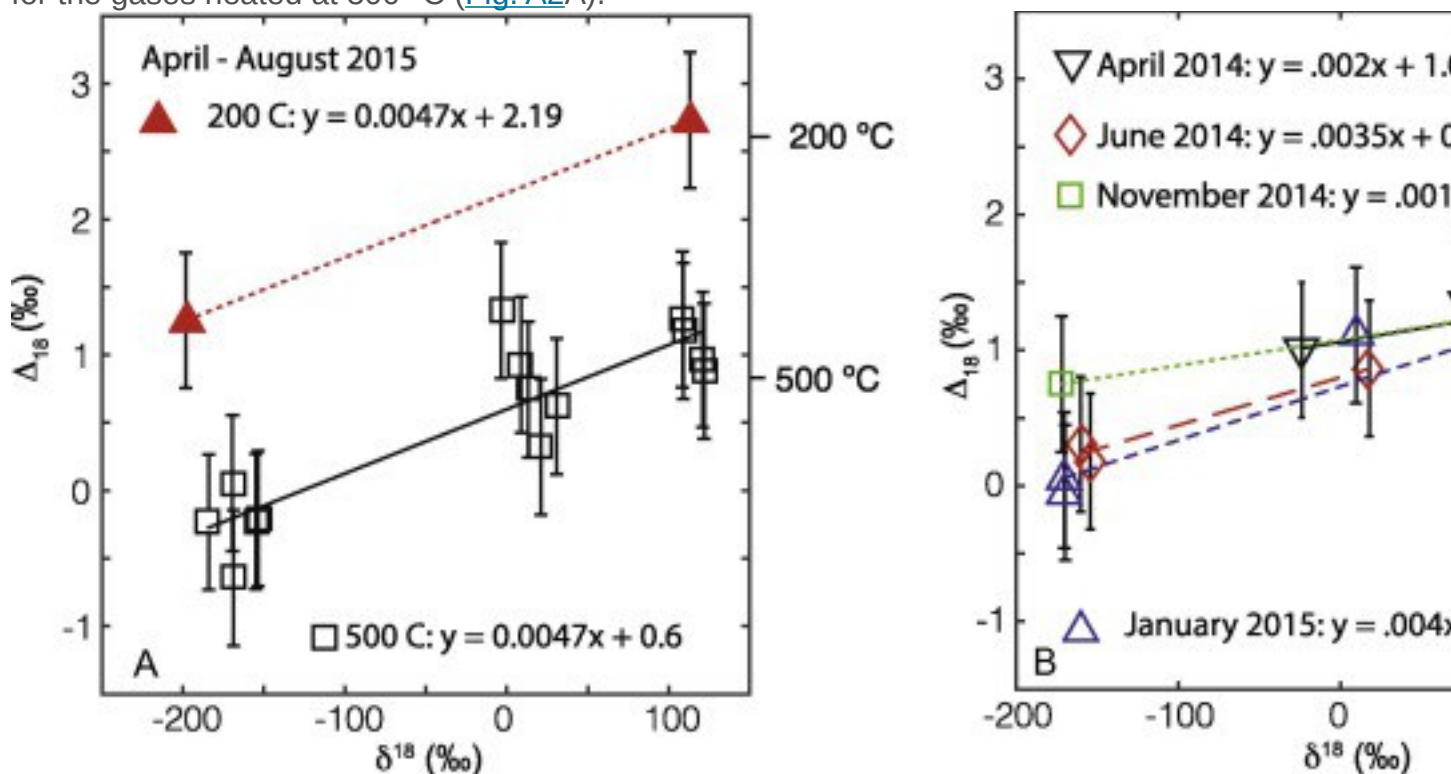
1. Download high-res image (283KB)
2. Download full-size image

Fig. A2. Plots of δ^{18} vs. Δ_{18} for heated methane standards, indicating the relationship between these values for (A) the measurement period from April to August 2015 when the dependence of Δ_{18} on δ^{18} was most clearly documented; and (B) for earlier

measurement periods. In (A) results for methane heated to both 500 and 200 °C are shown. Δ_{18}values equivalent to methane equilibration at 500 and 200 °C are shown on the right side of the plots. The average difference recovered for the 500 °C and 200 °C heated gases (1.59‰) is within 1 σ of the predicted difference based on the calibration given in Stolper et al. (2014a) (−1.78‰).

This effect appears to be similar to the dependence of Δ_{47} to bulk isotopic composition in CO_2 clumped isotope studies (Huntington et al., 2009, Dennis et al., 2011). We do not know the origin of this effect, but hypothesize it is related to background effects that were not present in previous studies or ion scrambling that has changed from the previous sessions. Based on this observed dependence of Δ_{18} on δ^{18} we applied a heated gas correction, similar to that applied in analyses of mass 47 CO_2 (Dennis et al., 2011), using the equation:

(A2)$\Delta 18HG = \Delta 18M - (\delta 18 \times m + b)$

where Δ_{18HG} is the corrected value, Δ_{18M} is the raw measured value, and m and b are slope and intercept parameters defined for each measurement period by the relationship between $\Delta_{18M}$and δ^{18} for heated gases (Fig. A2). Our basis for a constant set of parameters for a given measurement period is that the values for m and b remained constant over the course of the most recent, 15 week measurement period where the slope was most prominently observed (Fig. A2A). For the sake of internal consistency, and because doing so improved the reproducibility of samples analyzed in multiple measurement periods, we corrected all other measurement periods in this study following this protocol (Fig. A2B). We note, however, that the evidence for this dependence is not as strong in some of these measurement periods (Fig. A2B). For example, in one measurement period (April 2014) we did not measure a heated gas depleted in δ^{18} (δ^{18} < −20‰ relative to the internal reference standard). The heated gas correction is therefore less certain for this session for methane with δ^{18} values below −20‰. Subsequent replicate analyses of two samples measured in this measurement period (Goldstream Hotspot; Killarney Lake) indicate a 2SE uncertainty of 0.7‰. This uncertainty is larger than that of other replicate measurements, but does not affect the interpretation of these samples.

To ensure accuracy and precision of our measurements, especially in the context of the newly applied correction, the external precision of measurements was monitored by analyzing a standard differing in δD (+56‰), $\delta^{13}C$ (+33‰), and δ^{18} (+92‰) relative to the laboratory internal standard. External precision for Δ_{18} across all measurements was ±0.38‰ (1 standard deviation, σ; $n = 16$), and is offset in Δ_{18} by −0.06‰ from the long-term average of the standard over 2.5 years of measurements (1.6‰). The standard

deviation for measurements of this external standard was larger than previously observed in studies from this instrument (±0.19‰ in [Stolper et al., 2014b](#); ±0.23‰ in [Stolper et al. (2015)](#), for unknown reasons. For this reason we applied conservative, 2 SE uncertainties to our Δ_{18} values.

In two sessions we observed drift in the standard used to normalize data from a measurement session to a unified δD and Δ_{18} reference frame ([Stolper et al., 2014b](#)). We corrected for this drift by measuring the standard used for the correction multiple times over the course of these sessions and assumed the values required for sample correction changed linearly with time between observations of the standard. The quality of the correction was checked through multiple measurements of a secondary standard in all sessions and re-analysis of at least some samples in other sessions. For both sessions, average Δ_{18} values of the secondary standard were within 2 standard errors (2 SE) of its long-term average (Δ_{18} = 1.6): 1.54 ± 0.48 (n = 4) and 1.46 ± 0.18 (n = 11). Ten of the samples analyzed for this study were analyzed as replicates, in some cases in multiple measurement periods. The 2 SE standard error in Δ_{18} for these replicate analyses (n = 2 for all replicates) ranged between 0.03‰ and 0.80‰. The pooled standard deviation for replicate analyses (defined as the 1σ standard deviation of the residual of individual measurements from the sample mean) is 0.21‰.

Appendix 3: Details of isotopic mixing model

The mixing model presented in this study calculates the trends in plots of $\delta^{13}C$ vs. Δ_{18} and δD vs. Δ_{18} created by fractional mixing of specified end member [isotopic compositions](#). We performed these mixing model calculations using [isotope ratios](#) as the primary measure of composition (i.e., as opposed to δ or Δ values, which are less suitable as proxies for concentration in such models). Test calculations based on fractional isotopic abundance (a more accurate but laborious approach) were within error of the calculations performed with isotope ratios. The governing equations in our mixing model include, in addition to Eqs. [(1)](#), [(1)](#), [(1)](#) above:

(A3) $^{13}R_m = f_t \times {}^{13}R_t + (1-f_t) \times {}^{13}R_b$

(A4) $^{2}R_m = f_t \times {}^{2}R_t + (1-f_t) \times {}^{2}R_b$

(A5) $^{18}R_m = f_t \times {}^{18}R_t + (1-f_t) \times {}^{18}R_b$

where R_f, R_t, and R_m represent the isotope ratios of a given fractional mixture (m), or of the thermogenic (t) or biogenic (i.e. microbial; b) end-members, respectively, while superscript numbers denote the applicable isotopes. f_t is the fraction of thermogenic gas in a given mixture. While these terms imply a high-temperature thermogenic end-member, we note that a high-temperature microbial end-member is also possible.

The Δ_{18} mixing model assumes linear, conservative mixing of $\delta^{13}C$, and δD values between only two end-members (Fig. 7A). The assumption of only two end-members requires that end-member δD and $\delta^{13}C$ values fall along a mixing line defined by the sample δD and $\delta^{13}C$ values (Fig. 7A). This means that, for a given end-member $\delta^{13}C$ value, the end-member δD value is directly constrained by the δD–$\delta^{13}C$ mixing line. The thermogenic end-member δD and $\delta^{13}C$ values predicted by the $\Delta^{14}C$–$\delta^{13}C$ (Fig. 7C) and $\Delta^{14}C$–δD (not shown) mixing lines plots on the δD–$\delta^{13}C$ mixing line for Lake Eyak samples (Fig. 7A), which validates our approach. Note that there are different δD–$\delta^{13}C$ mixing lines depending on the inclusion of the PWS sample (Fig. 7A).

Using a Monte-Carlo approach, we randomly sampled 100,000 sets of $\delta^{13}C$ and Δ_{18} values, with a uniform distribution, for the thermogenic and microbial end-members, from a wide range of possible values (Fig. 7B). As discussed above, end-member δD values were directly constrained by end-member $\delta^{13}C$ values and were not specified. For the microbial end-member, Δ_{18} values were allowed to range from 8.4‰ (defined by sample Eyak-3) to −0.5‰ (the lowest value observed in a natural methane sample in this study; Table 2). Microbial end-member $\delta^{13}C$ values were allowed to range from −74‰ (defined by sample Eyak-3) to −120‰ (based on the empirical range of microbial methane $\delta^{13}C$; Whiticar et al., 1986). Thermogenic end-member Δ_{18} values were allowed to range from 6.2‰ (defined by sample Eyak-1) to 1.5‰ (an upper temperature limit of 300 °C; Quigley and Mackenzie, 1988, Clayton, 1991). Thermogenic end-member $\delta^{13}C$ values were allowed to range from −20‰ (an empirical upper limit for thermogenic methane; Whiticar et al., 1986) and −47‰ (defined by sample Eyak-1). We then calculated the resulting mixing lines in $\delta^{13}C$–Δ_{18} and δD–Δ_{18} space for each set of end-member compositions. A set of end-member values was determined to be acceptable if its mixing line passed within the 2 SE error of the $\delta^{13}C$–Δ_{18} and δD–Δ_{18} compositions of each of the sample measurements (Table 2). The acceptable sets of end-member values define $\delta^{13}C$–Δ_{18} (Fig. 8B) and δD–Δ_{18} (not shown) mixing lines.

References

Affek and Eiler, 2006

H.P. Affek, J.M. Eiler **Abundance of mass 47 CO$_2$ in urban air, car exhaust, and human breath**
Geochim. Cosmochim. Acta, 70 (2006), pp. 1-12
ArticleDownload PDFView Record in Scopus
Affek and Zaarur, 2014

H.P. Affek, S. Zaarur **Kinetic isotope effect in CO$_2$ degassing: insight from clumped and oxygen isotopes in laboratory precipitation experiments**

Geochim. Cosmochim. Acta, 143 (2014), pp. 319-330

ArticleDownload PDFView Record in Scopus

Affek et al., 2007

H.P. Affek, X. Xu, J.M. Eiler**Seasonal and diurnal variations of $^{13}C^{18}O^{16}O$ in air: initial observations from Pasadena, CA**

Geochim. Cosmochim. Acta, 71 (2007), pp. 5033-5043

ArticleDownload PDFView Record in Scopus

Affek et al., 2008

H.P. Affek, M. Bar-Matthews, A. Ayalon, A. Matthews, J.M.Eiler**Glacial/interglacial temperature variations in Soreq cave speleothems as recorded by 'clumped isotope' thermometry**

Geochim. Cosmochim. Acta, 72 (2008), pp. 5351-5360

ArticleDownload PDFView Record in Scopus

Anisimov, 2007

O. Anisimov**Potential feedback of thawing permafrost to the global climate system through methane emission**

Environ. Res. Lett., 2 (2007), p. 045016

CrossRef

Balabane et al., 1987

M. Balabane, E. Galimov, M. Hermann, R. Létolle**Hydrogen and carbon isotope fractionation during experimental production of bacterial methane**

Org. Geochem., 11 (1987), pp. 115-119

ArticleDownload PDFView Record in Scopus

Bernard et al., 1978

B.B. Bernard, J.M. Brooks, W.M. Sackett**Light hydrocarbons in recent Texas continental shelf and slope sediments**

J. Geophys. Res. Oceans, 83 (1978), pp. 4053-4061

CrossRef

Blair, 1998

N. Blair**The $\delta^{13}C$ of biogenic methane in marine sediments: the influence of C org deposition rate**

Chem. Geol., 152 (1998), pp. 139-150

ArticleDownload PDFView Record in Scopus

Borrel et al., 2011

G. Borrel, D. Jézéquel, C. Biderre-Petit, N. Morel-Desrosiers, J.-P. Morel, P. Peyret, G. Fonty, A.-C. Lehours**Production and consumption of methane in freshwater lake ecosystems**

Res. Microbiol., 162 (2011), pp. 832-847

ArticleDownload PDF

Bowen et al., 2007

G.J. Bowen, J.R. Ehleringer, L.A. Chesson, E. Stange, T.E. Cerling**Stable isotope ratios of tap water in the contiguous United States**
Water Resour. Res., 43 (2007)

Brosius et al., 2012

L. Brosius, Anthony
K. Walter, G. Grosse, J. Chanton, L.Farquharson, P.P. Overduin, H. Meyer**Using the deuterium isotope composition of permafrost meltwater to constrain thermokarst lake contributions to atmospheric CH$_4$ during the last deglaciation**
J. Geophys. Res. Biogeosci., 2005–2012 (2012), p. 117
CrossRef

Chanton et al., 2006

J.P. Chanton, D. Fields, M.E. Hines**Controls on the hydrogen isotopic composition of biogenic methane from high-latitude terrestrial wetlands**
J. Geophys. Res. Biogeosci., 2005–2012 (2006), p. 111

Christensen et al., 2004

T.R. Christensen, T. Johansson, H.J. Åkerman, M.Mastepanov, N. Malmer, T. Friborg, P. Crill, B.H. Svensson**Thawing Sub-arctic permafrost: effects on vegetation and methane emissions**
Geophys. Res. Lett., 31 (2004)

Clayton, 1991

C. Clayton**Carbon isotope fractionation during natural gas generation from kerogen**
Mar. Pet. Geol., 8 (1991), pp. 232-240
ArticleDownload PDFView Record in Scopus

J.C. Comiso, D.K. Hall**Climate trends in the Arctic as observed from space**

Wiley Interdiscip. Rev. Clim. Change, 5 (2014), pp. 389-409

CrossRefView Record in Scopus

R. Conrad**Quantification of methanogenic pathways using stable carbon isotopic signatures: a review and a proposal**

Org. Geochem., 36 (2005), pp. 739-752

ArticleDownload PDFView Record in Scopus

R. Conrad, M. Klose, P. Claus**Pathway of CH_4 formation in anoxic rice field soil and rice roots determined by ^{13}C-stable isotope fractionation**

Chemosphere, 47 (2002), pp. 797-806

ArticleDownload PDFView Record in Scopus

T.B. Coplen**Guidelines and recommended terms for expression of stable-isotope-ratio and gas-ratio measurement results**

Rapid Commun. Mass Spectrom., 25 (2011), pp. 2538-2560

CrossRefView Record in Scopus

R.E. Criss**Principles of Stable Isotope Distribution**

Oxford University Press, Oxford (1999)

L. Daniels, G. Fulton, R. Spencer, W. Orme-Johnson**Origin of hydrogen in methane produced by *Methanobacterium thermoautotrophicum***

J. Bacteriol., 141 (1980), pp. 694-698

View Record in Scopus

K.S. Dawson, D. Strąpoć, B. Huizinga, U. Lidstrom, M.Ashby, J.L. Macalady**Quantitative fluorescence in situ hybridization analysis of microbial consortia from a biogenic gas field in Alaska's Cook Inlet Basin**

Appl. Environ. Microbiol., 78 (2012), pp. 3599-3605

CrossRefView Record in Scopus

W. de Graaf, P. Wellsbury, R.J. Parkes, T.E.Cappenberg**Comparison of acetate turnover in methanogenic and sulfate-reducing sediments by radiolabeling and stable isotope labeling and by use of specific inhibitors: evidence for isotopic exchange**
Appl. Environ. Microbiol., 62 (1996), pp. 772-777
View Record in Scopus

Dennis et al., 20

K.J. Dennis, H.P. Affek, B.H. Passey, D.P. Schrag, J.M.Eiler**Defining an absolute reference frame for 'clumped' isotope studies of CO_2**
Geochim. Cosmochim. Acta, 75 (2011), pp. 7117-7131
ArticleDownload PDFView Record in Scopus

Eiler, 2013

J. Eiler**The isotopic anatomies of molecules and minerals**
Annu. Rev. Earth Planet. Sci., 41 (2013)

Eiler, 2007

J.M. Eiler**"Clumped-isotope" geochemistry – the study of naturally-occurring, multiply-substituted isotopologues**
Earth Planet. Sci. Lett., 262 (2007), pp. 309-327
ArticleDownload PDFView Record in Scopus

Eiler, 2011

J.M. Eiler**Paleoclimate reconstruction using carbonate clumped isotope thermometry**
Quatern. Sci. Rev., 30 (2011), pp. 3575-3588
ArticleDownload PDFView Record in Scopus

Eiler and Schaub

J.M. Eiler, E.A. Schauble**$^{13}C^{18}O^{16}O$ in earth's atmosphere**
Geochim. Cosmochim. Acta, 68 (2004), pp. 4767-4777
ArticleDownload PDFView Record in Scopus

Eiler et al., 2013

J.M. Eiler, M. Clog, P. Magyar, A. Piasecki, A. Sessions, D.Stolper, M. Deerberg, H.-J. Schlueter, J. Schwieters**A high-resolution gas-source isotope ratio mass spectrometer**
Int. J. Mass Spectrom., 335 (2013), pp. 45-56
ArticleDownload PDFView Record in Scopus

Feakins and Ses

S.J. Feakins, A.L. Sessions**Controls on the D/H ratios of plant leaf waxes in an arid ecosystem**
Geochim. Cosmochim. Acta, 74 (2010), pp. 2128-2141
ArticleDownload PDFView Record in Scopus

Fisher et al., 201

R.E. Fisher, S. Sriskantharajah, D. Lowry, M. Lanoisellé, C. Fowler, R. James, O. Hermansen, Myhre C. Lund, A. Stohl, J.Greinert, P.B.R. Nisbet-Jones, J. Mienert, E.G. Nisbet**Arctic methane sources: isotopic evidence for atmospheric inputs**
Geophys. Res. Lett., 38 (2011)

Formolo et al., 2

M. Formolo, J. Salacup, S. Petsch, A. Martini, K.Nüsslein**A new model linking atmospheric methane sources to Pleistocene glaciation via methanogenesis in sedimentary basins**
Geology, 36 (2008), pp. 139-142
CrossRefView Record in Scopus

Frederick and Bu

J. Frederick, B. Buffett**Taliks in relict submarine permafrost and methane hydrate deposits: pathways for gas escape under present and future conditions**
J. Geophys. Res. Earth Surf., 119 (2014), pp. 106-122
CrossRefView Record in Scopus

Ghosh et al., 200

P. Ghosh, J. Adkins, H. Affek, B. Balta, W.F. Guo, E.A.Schauble, D. Schrag, J.M. Eller^{13}C–^{18}O **bonds in carbonate minerals: a new kind of paleothermometer**
Geochim. Cosmochim. Acta, 70 (2006), pp. 1439-1456
ArticleDownload PDFView Record in Scopus

Graves et al., 20

C.A. Graves, L. Steinle, G. Rehder, H. Niemann, D.P.Connelly, D. Lowry, R.E. Fisher, A.W. Stott, H. Sahling, R.H. James**Fluxes and fate of dissolved methane released at the seafloor at the landward limit of the gas hydrate stability zone offshore western Svalbard**
J. Geophys. Res. Oceans (2015)

Holland and Bitz

M.M. Holland, C.M. Bitz**Polar amplification of climate change in coupled models**
Clim. Dyn., 21 (2003), pp. 221-232
CrossRefView Record in Scopus

Hornibrook et al.

E.R. Hornibrook, F.J. Longstaffe, W.S. Fyfe**Spatial distribution of microbial methane production pathways in temperate zone wetland soils: stable carbon and hydrogen isotope evidence**
Geochim. Cosmochim. Acta, 61 (1997), pp. 745-753
ArticleDownload PDFView Record in Scopus

Hornibrook et al.

E.R. Hornibrook, F.J. Longstaffe, W.S. Fyfe**Evolution of stable carbon isotope compositions for methane and carbon dioxide in freshwater wetlands and other anaerobic environments**
Geochim. Cosmochim. Acta, 64 (2000), pp. 1013-1027
ArticleDownload PDFView Record in Scopus

Hunt, 1979

M. Hunt**Petroleum Geochemistry and Geology**

WH Freeman and Company (1979)

Huntington et al.

K.W. Huntington, J.M. Eiler, H.P. Affek, W. Guo, M.Bonifacie, L.Y. Yeung, N. Thiagarajan, B. Passey, A. Tripati, M.Daeron, R. Came**Methods and limitations of 'clumped' CO_2 isotope (Δ_{47}) analysis by gas-source isotope ratio mass spectrometry**

J. Mass Spectrom., 44 (2009), pp. 1318-1329

CrossRefView Record in Scopus

Inagaki et al., 20

F. Inagaki, K.-U. Hinrichs, Y. Kubo, M. Bowles, V. Heuer, W.-L. Hong, T. Hoshino, A. Ijiri, H. Imachi, M. Ito, M. Kaneko, M.A.Lever, Y.-S. Lin, B.A. Methé, S. Morita, Y. Morona, W. Tanikawa, M.Bihan, S.A. Bowden, M. Elvert, C. Glombitza, D. Gross, G.J.Harrington, T. Hori, K. Li, D. Limmer, C.-H. Liu, N. Murayama, S.Ohkouchi, S. Ono, Y.-S. Park, S.C. Phillips, X. Prieto-Mollar, M.Purkey, N. Riedinger, Y. Sanada, J. Sauvage, G. Snyder, R.Susilawati, Y. Takano, E. Tasumi, T. Terada, H. Tomaru, E. Trembath-Reichert, D.T. Wang, Y. Yamada**Exploring deep microbial life in coal-bearing sediment down to ~2.5 km below the ocean floor**

Science, 349 (2015), pp. 420-424

CrossRefView Record in Scopus

Isaksen et al., 20

I.S. Isaksen, M. Gauss, G. Myhre, Walter K.M. Anthony, C. Ruppel**Strong atmospheric chemistry feedback to climate warming from Arctic methane emissions**

Global Biogeochem. Cycles, 25 (2011)

Jennings and Th

S. Jennings, G.R. Thompson**Diagenesis of Plio-Pleistocene sediments of the Colorado River delta, southern California**

J. Sediment. Res., 56 (1986)

Jones et al., 200

A.A. Jones, A.L. Sessions, B.J. Campbell, C. Li, D.L.Valentine**D/H ratios of fatty acids from marine particulate organic matter in the California Borderland Basins**

Org. Geochem., 39 (2008), pp. 485-500

ArticleDownload PDFView Record in Scopus

Kluge and Affek,

T. Kluge, H.P. Affek**Quantifying kinetic fractionation in Bunker Cave speleothems using Δ_{47}**

Quatern. Sci. Rev., 49 (2012), pp. 82-94

ArticleDownload PDFView Record in Scopus

Kort et al., 2012

E. Kort, S. Wofsy, B. Daube, M. Diao, J. Elkins, R. Gao, E.Hintsa, D. Hurst, R. Jimenez, F. Moore, J. Spackman, M. Zondlo**Atmospheric observations of Arctic Ocean methane emissions up to 82 °N**

Nat. Geosci., 5 (2012), pp. 318-321

[CrossRef](#)[View Record in Scopus](#)

[Koven et al., 201](#)

C.D. Koven, B. Ringeval, P. Friedlingstein, P. Ciais, P.Cadule, D. Khvorostyanov, G. Krinner, C. Tarnocai**Permafrost carbon-climate feedbacks accelerate global warming**

Proc. Natl. Acad. Sci. U.S.A., 108 (2011), pp. 14769-14774

[CrossRef](#)[View Record in Scopus](#)

[Krüger et al., 2002](#)

M. Krüger, G. Eller, R. Conrad, P. Frenzel**Seasonal variation in pathways of CH$_4$ production and in CH$_4$oxidation in rice fields determined by stable carbon isotopes and specific inhibitors**

Glob. Change Biol., 8 (2002), pp. 265-280

[CrossRef](#)[View Record in Scopus](#)

[Krzycki et al., 1987](#)

J. Krzycki, W. Kenealy, M. DeNiro, J. Zeikus**Stable carbon isotope fractionation by *Methanosarcina barkeri*during methanogenesis from acetate, methanol, or carbon dioxide–hydrogen**

Appl. Environ. Microbiol., 53 (1987), pp. 2597-2599

[View Record in Scopus](#)

[Lindgren et al., 2016](#)

R. Lindgren, G. Grosse, Anthony K. Walter, F. Meyer**Detection and spatiotemporal analysis of methane ebullition on thermokarst lake ice using high-resolution optical aerial imagery**

Biogeosciences, 13 (2016), pp. 27-44

[CrossRef](#)[View Record in Scopus](#)

[Martini et al., 1996](#)

A.M. Martini, J.M. Budai, L.M. Walter, M. Schoell**Microbial generation of economic accumulations of methane within a shallow organic-rich shale**

Nature, 383 (1996), pp. 155-158

[CrossRef](#)[View Record in Scopus](#)

[Matheus Carnevali et al., 2015](#)

P. Matheus Carnevali, M. Rohrssen, M.Williams, A. Michaud, H. Adams, D. Berisford, G. Love, J. Priscu, O.Rassuchine, K. Hand, A. Murray**Methane sources in Arctic thermokarst lake sediments on the North Slope of Alaska**

Geobiology, 13 (2015), pp. 181-197

[CrossRef](#)[View Record in Scopus](#)

[Meyer et al., 2010](#)

H. Meyer, L. Schirrmeister, A. Andreev, D. Wagner, H.-W.Hubberten, K. Yoshikawa, A. Bobrov, S. Wetterich, T. Opel, E.Kandiano, J. Brown**Lateglacial and Holocene isotopic and environmental history of northern coastal Alaska-Results from a buried ice-wedge system at Barrow**

Quatern. Sci. Rev., 29 (2010), pp. 3720-3735

[ArticleDownload PDFView Record in Scopus](#)

[Myhre et al., 2013](#)

G.D. Myhre, D. Shindell, F.-M. Bréon, W. Collins, J.Fuglestvedt, J. Huang, D. Koch, J.-F. Lamarque, D. Lee, B. Mendoza, T. Nakajima, A. Robock, G. Stephens, T. Takemura, H. Zhang**Anthropogenic and natural radiative forcing**

T.F. Stocker, G.-K. Qin, G.-K. Plattner, M. Tignor, S.K. Allen, J.Boschung, A. Nauels, Y. Xia, V. Bex, P.M. Midgley (Eds.), Climate Change 2013: The Physical Science Basis. Contribution of Working Group I to the Fifth Assessment Report of the Intergovernmental Panel on Climate Change, Cambridge University Press, Cambridge, U.K. (2013), pp. 659-740

[View Record in Scopus](#)

[O'Connor et al., 2010](#)

F.M. O'Connor, O. Boucher, N. Gedney, C. Jones, G.Folberth, R. Coppell, P. Friedlingstein, W. Collins, J. Chappellaz, J.Ridley, C. Johnson**Possible role of wetlands, permafrost, and methane hydrates in the methane cycle under future climate change: a review**

Rev. Geophys., 48 (2010)

[Ono et al., 2014](#)

S. Ono, D.T. Wang, D.S. Gruen, Lollar.B. Sherwood, M.Zahniser, B.J. McManus, D.D. Nelson**Measurement of a doubly-substituted methane isotopologue, $^{13}CH_3D$, by tunable infrared laser direct absorption spectroscopy**

Anal. Chem., 86 (2014), pp. 6487-6494

[CrossRefView Record in Scopus](#)

[Overduin et al., 2015](#)

P.P. Overduin, S. Liebner, C. Knoblauch, F. Günther, S.Wetterich, L. Schirrmeister, H.W. Hubberten, M.N. Grigoriev**Methane oxidation following submarine permafrost degradation: measurements from a central Laptev sea shelf borehole**

J. Geophys. Res. Biogeosci., 120 (2015), pp. 965-978

[CrossRefView Record in Scopus](#)

[Passey, 2015](#)

B.H. Passey**Biogeochemical tales told by isotope clumps**

Science, 348 (2015), pp. 394-395

[CrossRefView Record in Scopus](#)

[Paull et al., 2007](#)

C.K. Paull, W. Ussler, S.R. Dallimore, S.M. Blasco, T.D.Lorenson, H. Melling, B.E. Medioli, F.M. Nixon, F.A. McLaughlin**Origin of pingo-like features on the Beaufort Sea shelf and their possible relationship to decomposing methane gas hydrates**

Geophys. Res. Lett., 34 (2007)

Paull et al., 2011

C. Paull, S. Dallimore, J. Hughes-Clarke, S. Blasco, E.Lundsten, W. Ussler, D. Graves, A. Sherman, K. Conway, H. Melling, S. Vagle, T. Collett**Tracking the decomposition of submarine permafrost and gas hydrate under the shelf and slope of the Beaufort Sea**

7th International Conference on Gas Hydrates, Shell, Edinburgh, UK(2011)

Paull et al., 2015

C. Paull, S. Dallimore, D. Caress, R. Gwiazda, H. Melling, M. Riedel, Y. Jin, J. Hong, Y.G. Kim, D. Graves, A. Sherman, E.Lundsten, K. Anderson, L. Lundsten, H. Villinger, A. Kopf, S. Johnson, Clarke J. Hughes, S. Blasco, K. Conway, P. Neelands, H. Thomas, M.Côté**Active mud volcanoes on the continental slope of the Canadian Beaufort Sea**

Geochem. Geophys. Geosyst., 16 (2015), pp. 3160-3181

CrossRefView Record in Scopus

Penning et al., 2005

H. Penning, C.M. Plugge, P.E. Galand, R. Conrad**Variation of carbon isotope fractionation in hydrogenotrophic methanogenic microbial cultures and environmental samples at different energy status**

Glob. Change Biol., 11 (2005), pp. 2103-2113

CrossRefView Record in Scopus

Pine and Barker, 1956

M.J. Pine, H. Barker**Studies on the methane fermentation XII: the pathway of hydrogen in the acetate fermentation 1**

J. Bacteriol., 71 (1956), p. 644

View Record in Scopus

Portnov et al., 2013

A. Portnov, A.J. Smith, J. Mienert, G. Cherkashov, P.Rekant, P. Semenov, P. Serov, B. Vanshtein**Offshore permafrost decay and massive seabed methane escape in water depths >20 m at the South Kara Sea shelf**

Geophys. Res. Lett., 40 (2013), pp. 3962-3967

CrossRefView Record in Scopus

Prinzhofer and Pernaton, 1997

A. Prinzhofer, E. Pernaton**Isotopically light methane in natural gas: bacterial imprint or diffusive fractionation?**

Chem. Geol., 142 (1997), pp. 193-200

ArticleDownload PDFView Record in Scopus

Quigley and Mackenzie, 1988

T. Quigley, A. Mackenzie**The temperatures of oil and gas formation in the sub-surface**

Nature, 333 (1988), pp. 549-552

[CrossRefView Record in Scopus](#)

[Saenger et al., 2012](#)

C. Saenger, H.P. Affek, T. Felis, N. Thiagarajan, J.M.Lough, M. Holcomb**Carbonate clumped isotope variability in shallow water corals: temperature dependence and growth-related vital effects**

Geochim. Cosmochim. Acta, 99 (2012), pp. 224-242

[ArticleDownload PDFView Record in Scopus](#)

[Schoell, 1980](#)

M. Schoell**The hydrogen and carbon isotopic composition of methane from natural gases of various origins**

Geochim. Cosmochim. Acta, 44 (1980), pp. 649-661

[ArticleDownload PDFView Record in Scopus](#)

[Schuur et al., 2008](#)

E.A. Schuur, J. Bockheim, J.G. Canadell, E. Euskirchen, C.B. Field, S.V. Goryachkin, S. Hagemann, P. Kuhry, P.M. Lafleur, H.Lee, G. Mazhitova, F.E. Nelson, A. Rinke, V.E. Romanovsky, N.Shiklomanov, C. Tarnocai, S. Venevzky, J.G. Vogel, S.A. Zimov**Vulnerability of permafrost carbon to climate change: implications for the global carbon cycle**

Bioscience, 58 (2008), pp. 701-714

[CrossRefView Record in Scopus](#)

[Schuur et al., 2015](#)

E. Schuur, A. McGuire, C. Schädel, G. Grosse, J. Harden, D. Hayes, G. Hugelius, C. Koven, P. Kuhry, D. Lawrence, S. Natali, D.Olefeldt, V. Romanovsky, K. Schaefer, M. Turetsky, C. Treat, J. Vonk**Climate change and the permafrost carbon feedback**

Nature, 520 (2015), pp. 171-179

[CrossRefView Record in Scopus](#)

[Seewald, 2003](#)

J.S. Seewald**Organic–inorganic interactions in petroleum-producing sedimentary basins**

Nature, 426 (2003), pp. 327-333

[CrossRefView Record in Scopus](#)

[Shakhova et al., 2010](#)

N. Shakhova, I. Semiletov, A. Salyuk, V. Yusupov, D.Kosmach, Ö. Gustafsson**Extensive methane venting to the atmosphere from sediments of the East Siberian Arctic Shelf**

Science, 327 (2010), pp. 1246-1250

[CrossRefView Record in Scopus](#)

[Smith and Ingram-Smith, 2007](#)

K.S. Smith, C. Ingram-Smith*Methanosaeta*, **the forgotten methanogen?**

Trends Microbiol., 15 (2007), pp. 150-155

ArticleDownload PDFView Record in Scopus

Sowers et al., 1984

K.R. Sowers, S.F. Baron, J.G. Ferry*Methanosarcina acetivorans* **sp. nov., an acetotrophic methane-producing bacterium isolated from marine sediments**

Appl. Environ. Microbiol., 47 (1984), pp. 971-978

View Record in Scopus

Stolper et al., 2014a

D. Stolper, A. Sessions, A. Ferreira, Neto.E. Santos, A.Schimmelmann, S. Shusta, D. Valentine, J. Eiler**Combined ^{13}C–D and D–D clumping in methane: methods and preliminary results**

Geochim. Cosmochim. Acta, 126 (2014), pp. 169-191

ArticleDownload PDFView Record in Scopus

Stolper et al., 2014b

D. Stolper, M. Lawson, C. Davis, A. Ferreira, E.S. Neto, G. Ellis, M. Lewan, A. Martini, Y. Tang, M. Schoell, A.L. Sessions, J.M.Eiler**Formation temperatures of thermogenic and biogenic methane**

Science, 344 (2014), pp. 1500-1503

CrossRefView Record in Scopus

Stolper et al., 2015

D. Stolper, A. Martini, M. Clog, P. Douglas, S. Shusta, D.Valentine, A. Sessions, J. Eiler**Distinguishing and understanding thermogenic and biogenic sources of methane using multiply substituted isotopologues**

Geochim. Cosmochim. Acta, 161 (2015), pp. 219-247

ArticleDownload PDFView Record in Scopus

Strąpoć et al., 2011

D. Strąpoć, M. Mastalerz, K. Dawson, J. Macalady, A.V.Callaghan, B. Wawrik, C. Turich, M. Ashby**Biogeochemistry of microbial coal-bed methane**

Annu. Rev. Earth Planet. Sci., 39 (2011), pp. 617-656

CrossRefView Record in Scopus

Stuiver and Polach, 1977

M. Stuiver, H.A. Polach**Discussion; reporting of C-14 data**

Radiocarbon, 19 (1977), pp. 355-363

CrossRefView Record in Scopus

Sugimoto and Wada, 1995

A. Sugimoto, E. Wada**Hydrogen isotopic composition of bacterial methane: CO$_2$/H$_2$reduction and acetate fermentation**

Geochim. Cosmochim. Acta, 59 (1995), pp. 1329-1337

ArticleDownload PDFView Record in Scopus

Thornton et al., 2015

B.F. Thornton, M. Wik, P.M. Crill**Climate-forced changes in available energy and methane bubbling from Subarctic lakes**

Geophys. Res. Lett., 42 (2015), pp. 1936-1942

[CrossRef](#)[View Record in Scopus](#)

Tsuji et al., 2012

K. Tsuji, H. Teshima, H. Sasada, N. Yoshida**Spectroscopic isotope ratio measurement of doubly-substituted methane**

Spectrochim. Acta Part A Mol. Biomol. Spectrosc., 98 (2012), pp. 43-46

[Article](#)[Download PDF](#)[View Record in Scopus](#)

Urey and Rittenberg, 1933

H.C. Urey, D. Rittenberg**Some thermodynamic properties of the H1H2, H2H2 molecules and compounds containing the H2 atom**

J. Chem. Phys., 1 (1933), pp. 137-143

[CrossRef](#)[View Record in Scopus](#)

Valentine et al., 2004

D.L. Valentine, A. Chidthaisong, A. Rice, W.S.Reeburgh, S.C. Tyler**Carbon and hydrogen isotope fractionation by moderately thermophilic methanogens**

Geochim. Cosmochim. Acta, 68 (2004), pp. 1571-1590

[Article](#)[Download PDF](#)[View Record in Scopus](#)

Waldron et al., 1998

S. Waldron, I.A. Watson-Craik, A.J. Hall, A.E. Fallick**The carbon and hydrogen stable isotope composition of bacteriogenic methane: a laboratory study using a landfill inoculum**

Geomicrobiol J., 15 (1998), pp. 157-169

[CrossRef](#)[View Record in Scopus](#)

Waldron et al., 1999

S. Waldron, J. Lansdown, E. Scott, A. Fallick, A. Hall**The global influence of the hydrogen iostope composition of water on that of bacteriogenic methane from shallow freshwater environments**

Geochim. Cosmochim. Acta, 63 (1999), pp. 2237-2245

[Article](#)[Download PDF](#)[View Record in Scopus](#)

Walter Anthony and Anthony, 2013

Anthony K.M. Walter, P. Anthony**Constraining spatial variability of methane ebullition seeps in thermokarst lakes using point process models**

J. Geophys. Res. Biogeosci., 118 (2013), pp. 1015-1034

Walter Anthony et al., 2012

K.M. Walter Anthony, P. Anthony, G. Grosse, J.Chanton**Geologic methane seeps along boundaries of Arctic permafrost thaw and melting glaciers**

Nat. Geosci., 5 (2012), pp. 419-426

[CrossRef](#)[View Record in Scopus](#)

[Walter et al., 2006](#)

K.M. Walter, S. Zimov, J.P. Chanton, D. Verbyla, F.S.Chapin**Methane bubbling from Siberian thaw lakes as a positive feedback to climate warming**

Nature, 443 (2006), pp. 71-75

[CrossRef](#)[View Record in Scopus](#)

[Walter et al., 2008](#)

K.M. Walter, J.P. Chanton, F.S. Chapin, E.A.G. Schuur, S.A. Zimov**Methane production and bubble emissions from Arctic lakes: isotopic implications for source pathways and ages**

J. Geophys. Res. Biogeosci., 113 (2008)

[Wang et al., 2004](#)

Z.G. Wang, E.A. Schauble, J.M. Eiler**Equilibrium thermodynamics of multiply substituted isotopologues of molecular gases**

Geochim. Cosmochim. Acta, 68 (2004), pp. 4779-4797

[Article](#)[Download PDF](#)[View Record in Scopus](#)

[Wang et al., 2015](#)

D.T. Wang, D.S. Gruen, B.S. Lollar, K.-U. Hinrichs, L.C.Stewart, J.F. Holden, A.N. Hristov, J.W. Pohlman, P.L. Morrill, M.Könneke, K.B. Delwiche, E.P. Reeves, C.N. Sutcliffe, D.J. Ritter, J.S.Seewald, J.C. McIntosh, H.F. Hemond, M.D. Kubo, D. Cardace, T.M.Hoehler, S. Ono**Nonequilibrium clumped isotope signals in microbial methane**

Science, 348 (2015), pp. 428-431

[CrossRef](#)[View Record in Scopus](#)

[Webb and Miller, 2014](#)

M.A. Webb, T.F. Miller III**Position-specific and clumped stable isotope studies: comparison of the Urey and path-integral approaches for carbon dioxide, nitrous oxide, methane, and propane**

J. Phys. Chem. A, 118 (2014), pp. 467-474

[CrossRef](#)[View Record in Scopus](#)

[Westbrook et al., 2009](#)

G.K. Westbrook, K.E. Thatcher, E.J. Rohling, A.M.Piotrowski, H. Pälike, A.H. Osborne, E.G. Nisbet, T.A. Minshull, M.Lanoisellé, R.H. James, V. Hühnerbach, D. Green, R.E. Fisher, A.J.Crocker, A. Chabert, C. Bolton, A. Beszczynska-Möller, C. Berndt, A.Aquilina**Escape of methane gas from the seabed along the West Spitsbergen continental margin**

Geophys. Res. Lett., 36 (2009)

[Whiticar, 1999](#)

M.J. Whiticar**Carbon and hydrogen isotope systematics of bacterial formation and oxidation of methane**

Chem. Geol., 161 (1999), pp. 291-314

[Article](#)[Download PDF](#)[View Record in Scopus](#)

[Whiticar et al., 1986](#)

M.J. Whiticar, E. Faber, M. Schoell**Biogenic methane formation in marine and freshwater environments: CO$_2$ reduction *vs*. acetate fermentation—Isotope evidence**

Geochim. Cosmochim. Acta, 50 (1986), pp. 693-709

ArticleDownload PDFView Record in Scopus

Wik et al., 2013

M. Wik, P.M. Crill, R.K. Varner, D. Bastviken**Multiyear measurements of ebullitive methane flux from three Subarctic lakes**

J. Geophys. Res. Biogeosci., 118 (2013), pp. 1307-1321

CrossRefView Record in Scopus

Wik et al., 2016

M. Wik, R.K. Varner, Anthony K.M. Walter, S. MacIntyre, D.Bastviken**Climate-sensitive northern lakes and ponds are critical components of methane release**

Nat. Geosci., 9 (2016), pp. 99-105

CrossRefView Record in Scopus

Yeung et al., 2012

L.Y. Yeung, E.D. Young, E.A. Schauble**Measurements of $^{18}O–^{18}O$ and $^{17}O^{18}O$ in the atmosphere and the role of isotope-exchange reactions**

J. Geophys. Res. Atmos., 117 (2012)

Yeung et al., 2015

L.Y. Yeung, J.L. Ash, E.D. Young**Biological signatures in clumped isotopes of O$_2$**

Science, 348 (2015), pp. 431-434

CrossRefView Record in Scopus

Yoshinaga et al., 2014

M.Y. Yoshinaga, T. Holler, T. Goldhammer, G.Wegener, J.W. Pohlman, B. Brunner, M.M. Kuypers, K.-U. Hinrichs, M. Elvert**Carbon isotope equilibration during sulphate-limited anaerobic oxidation of methane**

Nat. Geosci., 7 (2014), pp. 190-194

CrossRefView Record in Scopus

$$\delta D = \left(\frac{{}^{2}R_{sample} - {}^{2}R_{VSMOW}}{{}^{2}R_{VSMOW}} \right) \quad\quad (1)$$

$$\delta^{13}C = \left(\frac{{}^{13}R_{sample} - {}^{13}R_{VPDB}}{{}^{13}R_{VPDB}} \right) \quad\quad (2)$$

where ${}^{2}R$ and ${}^{13}R$ are the ratios D/H and ${}^{13}C/{}^{12}C$ respectively. δD and $\delta^{13}C$ data are expressed as per mil (‰) values (Coplen, 2011).

Clumped isotope compositions are expressed using Δ_{18} notation (Stolper et al., 2014a):

$$\Delta_{18} = ({}^{18}R / {}^{18}R^{*} - 1) \quad\quad (3)$$

where

$$ {}^{18}R = ([{}^{13}CH_{3}D] + [{}^{12}CH_{2}D_{2}]) / [{}^{12}CH_{4}] \quad\quad (4)$$

The specified isotope ratios are measured from the corresponding ion beam current ratios, standardized by comparison with a standard of known composition. ${}^{18}R^{*}$ is the ${}^{18}R$ value expected for a random internal distribution of isotopologues, given the $\delta^{13}C$ and δD values of the sample (Stolper et al., 2014a), and is expressed as:

$$ {}^{18}R^{*} = \left(6 \times [{}^{2}R]^{2} \right) + \left(4 \times {}^{2}R \times {}^{13}R \right) \quad\quad (5)$$

The factors ('6' and '4') in Eq. (5) derive from the symmetry numbers of the mass 18 methane isotopologues (Stolper et al., 2014a). Δ_{18} data are reported as per mil (‰), where 0‰ refers to a random distribution of methane isotopologues (i.e., ${}^{18}R = {}^{18}R^{*}$). All samples are referenced against a laboratory

$$\Delta^{14}\mathrm{C} = \left(Fm * e^{\lambda(1950-Yc)} - 1 \right) \tag{7}$$

$$^{13}\alpha_{\mathrm{CO_2\text{-}CH_4}} = {}^{13}\mathrm{R_{CO_2}} / {}^{13}\mathrm{R_{CH_4}} \tag{8}$$

$$^{2}\alpha_{\mathrm{H_2O\text{-}CH_4}} = {}^{2}\mathrm{R_{H_2O}} / {}^{2}\mathrm{R_{CH_4}} \tag{9}$$

$$\delta^{18} = \left({}^{18}\mathrm{R_{sample}} / {}^{18}\mathrm{R_{standard}} - 1 \right) \tag{A1}$$

$$^{13}R_m = \left(f_t \times {}^{13}R_t \right) + \left((1 - f_t) \times {}^{13}R_b \right) \tag{A3}$$

$$^{2}R_m = \left(f_t \times {}^{2}R_t \right) + \left((1 - f_t) \times {}^{2}R_b \right) \tag{A4}$$

$$^{18}R_m = \left(f_t \times {}^{18}R_t \right) + \left((1 - f_t) \times {}^{18}R_b \right) \tag{A5}$$